The development of the adult nervous system in the annelid *Owenia fusiformis*

Allan M. Carrillo-Baltodano[1*], Rory Donnellan[1], Elizabeth A. Williams[2], Gáspar Jékely[3,4], José M. Martín-Durán[1]

[1]School of Biological and Behavioural Sciences, Queen Mary University of London, London, UK

[2]Faculty of Health and Life Sciences, University of Exeter, Exeter, UK

[3]Living Systems Institute, University of Exeter, Exeter, UK

[4]Centre for Organismal Studies (COS), University of Heidelberg, Heidelberg, Germany

[*]Corresponding author: a.carrillo-baltodano@qmul.ac.uk

Abstract

Background

The evolutionary origins of animal nervous systems remain contentious because we still have a limited understanding of neural development in most major animal clades. Annelids — a species-rich group with centralised nervous systems — have played central roles in hypotheses about the origins of animal nervous systems. However, most studies have focused on adults of deeply nested species in the annelid tree. Recently, *Owenia fusiformis* has emerged as an informative species to reconstruct ancestral traits in Annelida, given its phylogenetic position within the sister clade to all remaining annelids.

Methods

Combining immunohistochemistry of the conserved neuropeptides FVamide-lir, RYamide-lir, RGWamide-lir and MIP-lir with gene expression, we comprehensively characterise neural development from larva to adulthood in *Owenia fusiformis*.

Results

The early larval nervous system comprises a neuropeptide-rich apical organ connected through peripheral nerves to a prototroch ring and the chaetal sac. There are seven sensory neurons in the prototroch. A bilobed brain forms below the apical organ and connects to the ventral nerve cord of the developing juvenile. During metamorphosis, the brain compresses, becoming ring-shaped, and the trunk nervous system develops several longitudinal cords and segmented lateral nerves.

Conclusions

Our findings reveal the formation and reorganisation of the nervous system during the life cycle of *O. fusiformis*, an early-branching annelid. Despite its apparent neuroanatomical simplicity, this species has a diverse peptidergic nervous system, exhibiting morphological similarities with other annelids, particularly at the larval stages. Our work supports the importance of neuropeptides in animal nervous systems and the evolution of biphasic life cycles.

Keywords

Annelid, larvae, neuropeptides, nervous system.

Introduction

Nervous systems encompass all the neurons and their connections in an animal, representing an efficient way to communicate information along the body to elaborate behavioural and physiological responses in front of internal and external stimuli (1). Nervous systems are morphologically diverse, from diffuse nets as present in some non-bilaterian animals (e.g., ctenophores and cnidarians) to specialised and centralised systems with an anterior brain and post-cephalic longitudinal cords, as in many bilaterians (2, 3). Yet, how nervous systems evolved remains contentious because developmental information is lacking for many animal groups. Comparative, phylogenetically-guided studies on the specification, differentiation, patterning and architecture of nervous systems in as many different groups as possible (4, 5) are thus crucial to understand better how animal nervous systems originated and diversified (6).

Annelids — a group with a biphasic life cycle with a trochophore-like larva and centralised nervous systems as adults — have been central in understanding the evolution of nervous systems (3, 7-12). Traditionally, however, most studies have focused on species deeply nested in the annelid tree of life (13, 14), primarily on adults, and to a lesser extent using high-resolution developmental time courses (15-20). Therefore, studying lineages that branch off earlier in Annelida, such as Oweniidae, Magelonidae and Chaetopterimorpha, is essential to reconstruct ancestral traits in neural development for this animal clade (13, 21). Recent works in these groups (12, 21-26) have shown that a basiepidermal nervous system with a less organised brain was likely present in the last common annelid ancestor, which is a neuroanatomy that correlates well with their sedentary and tube-dwelling lifestyle (22). These studies have also indicated a simplification of the brain from larva to adult stages (22, 25, 26). However, we have previously demonstrated that the late embryos and early idiosyncratic

mitraria larvae of the Oweniid *Owenia fusiformis* (23) show signs of organised neurogenesis in the anterior neural system where the apical organ forms and in the ciliary band that works as the main locomotory organ (24). With feeding, the mitraria larva undergoes a series of morphological transformations and increases in size (23, 24, 27, 28), concurrent to significant changes in gene regulation and the formation of a juvenile rudiment that broadly corresponds to the future adult trunk (23, 24, 27-29). However, using only a few immunostaining markers has prevented a better understanding of neural development in *O. fusiformis*, particularly during metamorphosis.

In this study, we combine cross-species antibodies against a variety of highly-conserved neuropeptides (30-32) with gene expression analyses of anterior marker genes (9, 33, 34) to characterise the development of the nervous system in *O. fusiformis*, from the larval to the adult stages (Figure 1). Our findings reveal a transition from a bilateral bilobed brain before metamorphosis that fuses during metamorphosis to give rise to a ring-shaped brain in the adult. Likewise, it provides new evidence of the brain's connection with the future medullary cord of the trunk and the neural subdivisions in the segmented trunk. Together, we show a previously overlooked level of organisation of the nervous system in *O. fusiformis* that will be important to understanding the early dynamics of neural development in annelids and other animals.

Methods

Animal collection

Reproductive individuals of *O. fusiformis* were collected from the coast near the Station Biologique de Roscoff (France) and kept in the laboratory as previously described (24, 33). Embryos and larvae were cultured as previously described (24).

96

97 Immunohistochemistry

98 Fixation and antibody staining were conducted as described elsewhere (24). Adult
99 specimens were relaxed in 8% $MgCl_2$ and fixed overnight at 4°C. Adults were then placed in
100 60 mm dishes in 1x phosphate buffer saline (PBS), and their heads were dissected with a
101 razor blade between the thoracic and the abdominal segments (between segments three and
102 four (35, 36)). Adult heads were treated post-fixation with 1% collagenase D (Merk-Sigma, #
103 COLLD-RO) overnight at 4□°C and permeabilised through several washes with 1x PBS +
104 0.5% Triton X-100 (PTx). The primary antibodies mouse anti-acetylated α-tubulin (clone 6-
105 11B-1, Merk-Sigma, #MABT868, 1:800), mouse beta-tubulin (E7, Developmental Studies
106 Hybridoma Bank, 1:20), rabbit anti-FMRFamide (Immunostar, cat#: 20091, 1:600), and
107 *Platynereis dumerilii* derived (30-32) rabbit anti-FVamide (stock concentration: 0.12 mg/ml;
108 accession number: AEE25642.1, 1:200–1:500), anti-RYamide (stock concentration: 0.28
109 mg/ml; accession number: AEE25645.1, 1:200–1:500), anti-RGWamide (stock
110 concentration: 0.4 mg/ml; accession number: AFS33094.1, 1:200–1:500) and anti-MIP
111 (myoinhibitory peptide) (stock concentration: 0.28 mg/ml; accession number: AFV92893.1,
112 1:200–1:500) were diluted in 5% normal goat serum (NGS) in PTx and incubated overnight
113 at 4□°C. After several washes in 1% bovine serum albumin (BSA) in PTx, samples were
114 incubated with secondary antibodies AlexaFluor488, AlexaFluor555 and AlexaFluor647
115 conjugated antibodies (ThermoFisher Scientific, A-21428, A32731, A-21235, 1:600) plus
116 DAPI (stock 2mg/ml, 1:2000) diluted in 5% NGS in PTx overnight at 4□°C. Adults were
117 dehydrated stepwise in isopropanol, cleared in 2:1 benzyl benzoate:benzyl alcohol, briefly
118 immersed in xylene, and mounted in Entellan (Merk-Sigma, #1.07960).

119

120 Orthology analysis

A previously published alignment of SOX proteins (37) and maximum likelihood tree reconstruction with FastTree (38) were used to assign the orthology of SOXC in *O. fusiformis*.

Whole-mount in situ hybridisation

Riboprobes were synthesised with the T7 enzyme following the manufacturer's recommendations (Ambion's MEGAscript kit, #AM1334) and stored in hybridisation buffer at a concentration of 50 ng/µl at −20°C. Single colourimetric *in situ* hybridisation of embryos and mitraria larvae was performed following an established protocol using a 1.5 ng/µl probe concentration (24, 29, 33, 34).

Imaging

Representative embryos, larvae, and juveniles from the colourimetric whole mount *in situ* hybridisation experiments were cleared and mounted in 80% glycerol in PBS. They were imaged with a Leica DMRA2 upright microscope equipped with an Infinity5 camera (Lumenera) using differential interference contrast (DIC) optics. Confocal laser scanning microscopy (CLSM) images were taken with a Leica SP5, Leica Stellaris 8 and Nikon CSU-W1 spinning disk confocal microscope. CLSM Z-stack projections were built with ImageJ2 (39) and Nikon NIS-elements software. DIC images were digitally stacked with Helicon Focus 7 (HeliconSoft). Brightness and contrast were edited with Adobe Photoshop CC (v 24.0.0), and figures were built with Adobe Illustrator CC (v 27.0.0) (Adobe Inc.).

Results

To characterise better the complexity and development of the nervous system of *O. fusiformis*, we tested four purified antibodies against conserved mature neuropeptides

(FVamide, RYamide, RGWamide and MIP) of the annelid *P. dumerilii* that have broad cross-species immunoreactivity (Figure 1b–c; Figure 2; Additional File 1: Supplementary Figure 1; Additional File 2: Supplementary Figure 2) (30, 32, 40). FVamide, RYamide and RGWamide label many of the previously described components of the early larval nervous system (24) (Figure 2), including the apical organ and the prototroch ring, but also previously uncharacterised peripheral nerves in the larval episphere. The MIP antibody has a lower signal-to-noise ratio but still labels the apical organ and some tissue anterior to the larval mouth (Additional File 2: Supplementary Figure 2). Having confirmed their connection to the larval neural components, we focused on describing the immuno-reactivity of these antibodies during the life cycle of *O. fusiformis*, using tubulin as a counter-immunostaining of the nervous system.

The complex nervous system of the early mitraria

At 24 hours post-fertilisation (hpf), between three to seven FVamide-like immune-reactive (FVamide-lir), RYamide-lir and RGWamide-lir cells are detectable in the apical organ of the early mitraria larva (Figure 2). A solitary FVamide-lir neuron with a weak FVamide-lir short axon is positioned anterior and apical to the mouth (white arrow, Figure 2a–b). MIP has a similar pattern of immunoreactivity (white arrow, Additional File 2: Supplementary Figure 2). RYamide-lir axons, on the other hand, connect the apical organ to an RYamide-lir prototroch ring (pr) (magenta arrowhead, Figure 2e–f, h) via a frontal nerve (fn), a dorsal nerve (dn) and two bilateral peripheral nerves (lpn1–2) that bifurcate further midway in the episphere (orange arrowheads, Figure 2e–f). The prototroch ring also contains seven RYamide-lir cells (magenta arrows, Figure 2e–f, h–i), three anterior and four posterior, similar to the FMRFamide-lir, *elav*$^{+}$ and *synaptotagmin*$^{+}$ cells previously described at this larval stage (24). In contrast, RGWamide-lir cells are exclusively restricted to the apical

organ (Figure 2j–l). Apical cilia protrudes from some of the FVamide-lir, RYamide-lir, RGWamide-lir and MIP-lir neurons of the apical organ (Figure 2b, e, j; Additional File 2: Supplementary Figure 2). At this stage, beta-tubulin and alpha-acetylated tubulin label the frontal, dorsal, and peripheral nerves connecting the apical organ with the tubulin^{+} prototroch ring (Figure 3a–e, h–m). Near the seven refringent globules of unknown function (24, 27), but integrated within the prototroch, are at least five beta-tubulin^{+} monociliated cells with a short cilium, which likely represent mechanoreceptors (Figure 3e–g). Together, these new neuropeptide antibodies and more detailed observations of tubulin immunostaining demonstrate the complexity of the apical organ and neural components of the prototroch, including elaborated neurite patterns that connect these two sensorial structures, many of which had been previously overlooked (9, 23, 24).

The formation of the brain and nerve cords

As the larva grows and acquires competence, the adult brain forms, first as a horseshoe-shaped, bilobular, apical condensation of nuclei recognisable, as well, through the cell membrane labelling with beta-tubulin (27) (br; Figure 4a, e, g, k, m, o, q, u; Additional File 3: Supplementary Figure 3a, d, g, j; Additional File 4: Supplementary Figure 4a–d). In addition, the bilateral gene expression of the putative neural gene *soxC* (Additional File 5: Supplementary Figure 5) and anterior markers *pou4*, *six3/6*, *nk2.1* and *ChAt* (Figure 5a–f, i–l) confirm the bilobular nature of the brain at this stage. A small pit, as referred to by Wilson (27), is positioned most apically in the brain, where the ciliated apical tuft protrudes (Additional File 4: Supplementary Figure 4a–b, g–i). In addition, an apical ring of FVamide-lir, RYamide-lir, MIP-lir, and tubulin^{+} cells surround this apical tuft (ar; Figure 4f, j, v; Additional File 4: Supplementary Figure 4b, h) and is presumably part of the apical organ. At this stage, this neural larval organ also contains multiple FVamide-lir, RYamide-lir,

196 RGWamide-lir and MIP-lir neurons, interconnected with the brain sitting just below (ao;
197 Figure 4 a–b, d–f, g–l, m–r, u–v; Additional File 3: Supplementary Figure 3). Two thick
198 RYamide-lir and tubulin^{+} axon bundles — the ventral and dorsal roots — cross the brain and
199 form a central neuropil just below the condensed nuclei of the brain (23, 27) (Figure 4k–l;
200 Additional File 4: Supplementary Figure 4c, h). We used the terms “ventral” root and
201 “dorsal” root to follow the nomenclature of the brain in other annelids (14, 41). However, the
202 ventral and dorsal roots are positioned anteriorly and posteriorly, respectively, along the main
203 body axis of the larva and juvenile. Altogether, these apical neural structures connect with the
204 developing ventral nerve cord (vnc) of the juvenile rudiment (see below) through FVamide-
205 lir, MIP-lir (Additional File 3: Supplementary Figure 3b, k), and tubulin^{+} (Additional File 4:
206 Supplementary Figure 4b) circumesophageal connectives. Eyespots are present on each side
207 of the most basal part of the brain (not shown) (23, 27). Lastly, frontal and dorsal nerves, plus
208 the lateral peripheral nerves, maintain the connection between the apical organ/brain and the
209 prototroch neural ring (Figure 4b, h, r; Additional File 3: Supplementary Figure 3b, e, k;
210 Additional File 4: Supplementary Figure 4f, i).
211
212 At this pre-metamorphic larval stage, the juvenile rudiment has grown into a defined
213 trunk, with segments that will wrap around the gut as it prepares to evaginate from the larval
214 body (27-29). The vnc of the trunk starts forming as early as two weeks post fertilisation
215 (wpf) and is immunoreactive to serotonin (5HT), FMRFamide and tubulin (23). Between two
216 to three wpf, 5HT-lir and FMRFamide-lir neurons and lateral nerves presumably get
217 patterned on each of the developing trunk segments (23). In agreement with the expression of
218 *elav* and *synaptotagmin*, *soxC* is highly expressed in the juvenile trunk at this stage,
219 supporting that this is a prominent site of active neurogenesis in the competent larva (24)
220 (Figure 5a–b). Not only has the trunk an FVamide-lir, RYamide-lir, MIP-lir and tubulin^{+} vnc

but also an FVamide-lir and RYamide-lir dorsal one (Additional File 3: Supplementary Figure 3c, f), demonstrating that many of the components of the adult peripheral nervous system develop before metamorphosis.

In addition to the developing brain and nerve cords, the foregut is innervated with FVamide-lir and RYamide-lir neurons and nerves (fgn; Figure 4d–d, h; Additional File 3: Supplementary Figure 3b–c, e–f). MIP shows some unspecific labelling at the anterior section of the foregut (Figure 4s–t; Additional File 3: Supplementary Figure 3k–l), mirroring the expression domains of *soxC*, *otx*, *nk2.1*, and *ChAt* in this larval region (Figure 5a, g, i, k). Dorsal to the posterior tip of the trunk, the larval chaetal sac, which has many more chaetae at this stage than in the early mitraria, has an RYamide-lir and MIP-lir nerve connecting these defensive structures to the peripheral neurites of the episphere (Additional File 3: Supplementary Figure 3f, l). Altogether, the comprehensive analysis of the nervous system of the competent larva of *O. fusiformis* reveals a transition of neural connectivity, where the forming adult brain remains connected to the transitory larval organs, such as the prototroch and chaetal sac, as the connections with the developing trunk nervous system are established.

The nervous system during metamorphosis

The apical organ remains positioned dorsally and apically to the double root of axons of the brain (i.e., the central neuropil; Figure 6; Additional File 6: Supplementary Figure 6a), and continues to be connected with the larval episphere and prototroch ring with the FVamide-lir, RYamide-lir and tubulin^{+} dorsal nerves (Additional File 6: Supplementary Figure 6a–d; Additional File 7: Supplementary Figure 7b), and RYamide-lir and tubulin^{+} lateral nerves (Figure 6c–d; Additional File 6: Supplementary Figure 6c–d; Additional File 6: Supplementary Figure 7a–b). The distinct two lobes of the brain of the competent larva

appear to fuse into a continuous horseshoe during metamorphosis (Figure 7b, f), forming the putative ring-shaped brain of the juvenile and adult (see below). The dorsal and ventral root of the brain creates an FVamide-lir, RYamide-lir, RGWamide-lir, MIP-lir and tubulin^{+} neuropil (np; Figure 6c, f, i, l; Additional File 7: Supplementary Figure 7a–b), which connects to the thorax of the evaginating trunk via circumesophageal connectives (or lateral medullary cords (22); see discussion) (Figure 6; Additional File 6: Supplementary Figure 6; Additional File 7: Supplementary Figure 7a–b). In the juvenile and adult, the thorax is composed of three fused trunk segments, which we name ciliated thoracic segments (cts), and differentiate from the other trunk segments by having capillary chaetae (35, 36) and abundant cilia in the epidermis (Additional File 7: Supplementary Figure 7a–b). Paired RGWamide-lir parapodial glandular organs (pgos) up to the seventh segment (27, 42) facilitate the distinction between the three thoracic and the seven abdominal segments (27, 28) (Figure 6g–h; Additional File 6: Supplementary Figure 6e–f). We could not observe ganglia in either thoracic or abdominal segments using nuclear staining and gene expression (Figure 7), providing further evidence of the medullary cord nature in oweniids (12, 22). However, several iterated FVamide-lir, RYamide-lir, RGWamide-lir, and MIP-lir neurons are present along the vnc, which are more condensed in the thorax because of the fusion of the three thoracic segments and more distant in the rest of the trunk (Figure 6a–b, d–e, g–h, j–k; Additional File 6: Supplementary Figure 6). From these clusters of iterated neurons, FVamide-lir, RYamide-lir, RGWamide-lir, MIP-lir and tubulin^{+} lateral nerves run on the anterior edge of each segment transversally towards the dorsal side of the trunk, connecting to the dorsal nerve cord (Additional File 6: Supplementary Figure 6; Additional File 7: Supplementary Figure 7b). During metamorphosis, the foregut will break from the larval tissue to connect with the brain and become the definite mouth of the juvenile (27). The patterns of innervation and gene expression remain very similar to that of the competent

larvae (compare Figure 5 with Figure 7, and Additional File 3: Supplementary Figure 3 with Additional File 6: Supplementary Figure 6), except that now there are RGW-lir neurons on the lower mouth lip (lml; Figure 6g–h; Additional File 6: Supplementary Figure 6e–f). At this stage, *soxC* is broadly expressed in the mouth, and *six3/6* and *nk2.1* are expressed in the dorsal part of the foregut. *Otx* is now expressed in the boundary between the foregut and the midgut (Figure 7a–b, e–f, g–j), suggesting an additional role in the neural innervation of the foregut. Altogether, our findings indicate that significant changes in the neural architecture occur during metamorphosis, as the originally bilobed brain transforms into a ring and connects with the anterior part of the trunk, establishing the final nervous system architecture of the juvenile/adult.

The juvenile nervous system

After metamorphosis, the juvenile body subdivides into the head — with the fused prostomium and peristomium — and the trunk, further differentiating into three fused thoracic segments, seven abdominal segments, and the pygidium (27) (Figure 8). The mouth is anterior, and the brain ring is positioned dorsal to the roof of the foregut (23). The brain ring comprises 5HT-lir, FMRFamide-lir, and tubulin^{+} roots, connected via lateral medullary cords around the foregut to the vnc (9, 12, 23). The vnc has iterated 5HT-lir neurons in an otherwise continuous medullary cord with no breaks, as seen with *ChAt* expression (9, 12, 23). Consistently, FVamide-lir, RYamide-lir, RGWamide-lir, and MIP-lir localise to the ring-shaped brain that connects to the vnc with lateral medullary cords at the ciliated thoracic segments (Figure 8). FVamide-lir and RYamide-lir clusters of neurons (Figure 8a–d) and FVamide-lir, RYamide-lir, and tubulin^{+} peripheral nerves (Additional File 7: Supplementary Figure 7c–d) occur in the anterior part of each segment, with one tubulin^{+} pair of lateral nerves more prominent in each of the segments (ln; Additional File 7: Supplementary Figure

296 7c–d). Tubulin^{+} longitudinal nerve tracts run alongside the median vnc (cyan arrows;
297 Additional File 7: Supplementary Figure 7c) and ventrolaterally (magenta arrows; Additional
298 File 7: Supplementary Figure 7c–d). RGWamide-lir and MIP-lir nerves are also present in the
299 mouth opening (Figure 8e–h). At this stage, *six3/6* and weakly *soxC* are expressed in the
300 brain (Additional File 8: Supplementary Figure 8a–f). The latter is also expressed in the
301 foregut and the putative posterior growth zone (gz), just before the pygidium (Additional File
302 8: Supplementary Figure 8a–c). Therefore, the definitive brain is primarily formed in the
303 juvenile. However, the vnc neuroarchitecture is more elaborated at this stage than in the
304 adult, as we describe below (12, 22).
305
306 The anterior adult neural structures
307 The head of the adult *O. fusiformis* includes a crown of tentacles formed from the
308 fused prostomium and peristomium and a pair of ventrolateral eyes (22, 36) (Figure 9a). The
309 FVamide-lir, RYamide-lir, RGWamide-lir, and MIP-lir nervous system is preserved
310 throughout the ring-shaped brain, medullary cords, and vnc as seen in the juvenile (Figure 9;
311 Additional File 9: Supplementary Figure 9). The neuropile of the brain is composed of
312 parallel bundles of axons transverse to the lateral medullary cords, with FVamide-lir,
313 RYamide-lir, RGWamide-lir, and MIP-lir neurons on the anterior and posterior edges (Figure
314 9b, d, f, h; Additional File 9: Supplementary Figure 9c, f, i, l). The FVamide-lir and
315 RYamide-lir neuropil is wider than the RGWamide-lir and MIP-lir. The RYamide-lir neurons
316 of the neuropil partially distinguish the dorsal and ventral roots of the brain as two
317 concentrated bundles of neurites parallel to one another, separated by a less dense portion of
318 neurites (Additional File 9: Supplementary Figure 9f), suggesting some level of
319 compartmentalisation in the apparently simple ring-shaped brain of this annelid. Finally,
320 there are FVamide-lir, RYamide-lir, RGWamide-lir, and MIP-lir longitudinal head nerves

lateral to the brain (Additional File 9: Supplementary Figure 9b, f, j, n) that project anteriorly to the tentacles (22), and posteriorly into the trunk.

In addition to the brain, FVamide-lir, RYamide-lir, RGWamide-lir, and MIP-lir somata are present throughout the head tentacles (Figure 9 a–h) and surrounding the eyes (Figure 9a, c, e, g; Additional File 9: Supplementary Figure 9a, d, g, j). In these visual organs, a posterolateral cluster of neurons exhibits primarily FVamide-lir but also some RYamide-lir and MIP-lir signal, while RYamide-lir dominates in a second anterior cluster, which also shows some FVamide-lir and MIP-lir (Figure 9a, c, g; Additional File 9: Supplementary Figure 9a, d, j). However, this immunoreactivity is not part of the eye structure (21). A dorsal nerve cord composed of FVamide-lir, RYamide-lir, RGWamide-lir, and MIP-lir neurites and somata extends across the dorsal side of the body (Additional File 9: Supplementary Figure 9b, e, h, k). Some of these immunoreactivity patterns in the head support previously observed 5HT-lir and FMRFamide-lir clusters in other oweniids (43, 44). Our findings support that the adult brain and trunk nervous system are compartmentalised during the gradual reorganisation of the nervous system from larval and juvenile stages.

Discussion

This study characterises the ontogeny of the nervous system in *O. fusiformis* from larvae to adulthood using a set of conserved cross-species antibodies and gene expression. The morphological landmarks presented here will serve as a foundation to understand larval development, metamorphosis, and post-larval morphogenesis in an annelid occupying a critical phylogenetic position, which will help to infer ancestral characters to Annelida and animals in general (Figure 10).

346 The nervous system in the early larva

347 The mitraria larva largely derives from anterior/head tissues (29), and posterior
348 territories are limited to a ventral epithelial invagination that will form the juvenile rudiment
349 trunk (24, 27) and a small dorsal posterior tissue that includes the anus and chaetal sac (34).
350 The larval neural system — composed of the apical organ and apical tuft connected to a
351 prototroch ring — starts developing by 13 hours post fertilisation (hpf) and connects to the
352 FMRFamide-lir prototroch ring by 24 hpf. The nervous system also includes seven
353 FMRFamide-lir, *elav*$^{+}$ and *synaptotagmin*$^{+}$ neurons in the prototroch (24). Our findings
354 support this early neural architecture of the mitraria larva and reveal further complexity and
355 refinement, particularly in the apical organ and its connections to the prototrochal neural ring.
356 As in *P. dumerilii*, the apical organ contains FVamide-lir, RYamide-lir, RGWamide-lir, and
357 MIP-lir neurons in *O. fusiformis*, some of which are monociliated. All these neuropeptides
358 form a neurosecretory centre that regulates the swimming behaviour of the larvae of *P.*
359 *dumerilii* (31, 32, 45, 46). They are also present in the anterior neural systems of other
360 annelid and spiralian larvae, as in *C. teleta*, and even directly developing species (30-32, 40).
361 In *O. fusiformis*, the apical organ connects frontally, bilaterally, and dorsally to the prototroch
362 (Figure 10a). The monociliary nature of the neuropeptide-lir neurons in the apical organ and
363 the seven RYamide-lir neurons in the prototroch indicate they might have a sensory function
364 (Figure 10a). They presumably integrate stimuli from the apical organ and the prototroch to
365 control the shape of the episphere and the ciliary beating, thus influencing the locomotion and
366 behaviour of the larva, without the need for excess neural wiring as hypothesised for larvae
367 with monociliated cells (47).
368
369 The spatial patterns of immunoreactivity show notable similarities between *O.*
370 *fusiformis* and *P. dumerilii*. In both larvae, RY (31), FV (30, 31, 48, 49), and MIP (32, 48-50)

occur in ciliated sensory neurons. However, RY and RGW are expressed in interneurons that communicate to the synaptic nervous system in *P. dumerilii* (48, 49, 51, 52). Future studies of the connectome in *O. fusiformis* could clarify if this is true for *O. fusiformis*. Nonetheless, the presence of diverse neuropeptide sensory neurons, together with the deployment of staggered apical expression domains of transcription factors like *foxQ2*, *six3/6* and *otx* (11, 33, 53), support the evolutionary conservation of the apical region between annelids and spiralians and reveal anatomical traits of the anterior neural system of the ancestral "head swimming larva" of annelids.

From a bilobed larval brain to an adult ring-shaped brain

With growth, the neural features present in the early larva become more elaborated (23, 24), and the adult nervous system develops, first with the condensation of nuclei that form the brain (Figure 10b) and later, with the patterning, elongation and subsequent evagination of the trunk. Nuclear staining, the expression of the anterior marker genes *ChAt*, *nk2.1*, *otx*, *pou4*, and *six3/6* (9, 33, 34), and neuropeptide immunoreactivity reveal that the pre-metamorphic larva has a bilobed brain (Figure 10b). This is consistent with classic morphological descriptions (27) and similar to the larvae of other "early branching" (54, 55) and more divergent annelids (15, 16, 56). The brain sits underneath a prominent neuropeptide-rich apical organ (Figure 10b), which comprises an apical ring and several neurons surrounding the monociliated apical tuft. Anterior and posterior FMRFamide-lir and 5HT-lir (23) and RYamide-lir axonal roots form a neuropil underneath the brain referred to as ventral and dorsal roots in other annelids, respectively (14, 41). Remarkably, this organisation changes with metamorphosis, as the bilobed brain forms a continuous *soxC+* and *six3/6+* band that compresses anteroposteriorly, bringing the dorsoventral roots closer to each other (Figure 10b). This results in the fusion of the brain lobes and roots into a double ring that

396 forms the brain in the juvenile (23) and adult (22). While our data support a reorganisation of
397 the brain from larval to adult stages (22, 25, 26), we were unable to determine the fate of the
398 larval apical organ, and it remains unclear whether it integrates into the juvenile brain or is
399 resorbed during metamorphosis with the apical tuft and prototroch.
400
401 From metamorphosis onwards, the roots of the brain neuropil connect with lateral
402 medullary cords, ending into a medullary non-ganglionated, medially-condensed vnc in the
403 trunk (12, 22). The presence of bundles of axons with distinct neuropeptide immunoreactivity
404 in the adult brain ring suggests an unexpected level of compartmentalisation in this
405 previously regarded "simple" brain (22) that might indicate the retention of the anterior and
406 posterior roots ("ventral" and "dorsal", respectively, according to traditional anatomical
407 descriptions (14, 41)) seen in the larval and metamorphic stages in adult stages. This would
408 challenge hypotheses based on the analysis of other oweniids that their ring-shaped brain is
409 homologous to the dorsal (posterior) root neuropil of other annelids (43, 44). Despite its
410 presumable compartmentalisation, there are no distinct ganglionic centres in the adult brain
411 of *O. fusiformis*, unlike in more active annelids that exhibit structures like the mushroom
412 bodies and nuchal organs (57, 58). Therefore, the brains of *O. fusiformis* and other
413 representatives of the "early branching" clades gradually reorganise their morphology while
414 retaining neuronal diversity during metamorphosis to form a continuous medullary cord with
415 the vnc, perhaps associated with a transition to a more sedentary, tube-dwelling lifestyle as
416 adults.
417
418 <u>From a juvenile rudiment to the trunk nervous system</u>
419 The trunk of oweniids forms as an invagination of the ventral epithelium of the larva
420 (27, 28) with the deployment of conserved anterior-posterior and trunk-patterning

421 programmes like the *hox* genes (29). While neurogenesis, as revealed by the expression of
422 *elav*, *synaptotagmin* (24), and *soxC* (this study), is predominant in the apical organ and brain
423 region in the early larva, it mainly occurs in the developing trunk before metamorphosis. As
424 in other annelids (9, 12), the trunk nervous system develops as a paired medially-condensed
425 vnc, but, most notably, it also includes a single dorsal nerve cord connected to the ventral one
426 by segmentally iterated lateral nerves. During metamorphosis, additional ventrolateral
427 longitudinal cords form, giving the trunk nervous system an orthogonal appearance that has
428 been hypothesised to be the ancestral pattern for annelids (59) and other spiralians, such as
429 flatworms and nemerteans (60, 61). A ganglionated ladder-like vnc thus likely evolved
430 independently multiple times in annelids and animals (9, 12). As the juvenile worm matures
431 into adulthood, more neurons appear along the vnc, resulting in a continuous medullary cord
432 with no apparent breaks (12, 22, 43). However, the lack of segmented ganglia in the vnc of *O.*
433 *fusiformis* does not exclude the presence of clusters of 5HT-lir (9, 12, 23) and FVamide-lir,
434 RYamide-lir and MIP-lir (this study) neurons in each segment. Parapodial glandular organs
435 (PGOs) (42) develop in each of the first seven segments (27) and show RGWamide-lir, which
436 combined with the cilia of the thoracic segments and the neuropeptide-lir and tubulin^{+} lateral
437 nerves of the abdominal segments, define positional landmarks along the anterior-posterior
438 axis that would aid in the study of trunk formation in *O. fusiformis* (Figure 10c). Concurrent
439 with the maturation of the brain and trunk nervous system, the immunoreactivity in the larval
440 foregut and definitive oesophagus changes. In *O. fusiformis*, the foregut of the competent
441 larvae is innervated by 5HT-lir and FMRFamide-lir (23, 24), and FVamide-lir and RYamide-
442 lir neurons and axons (this study); and by 5HT-lir (23) and RGWamide-lir and MIP-lir (this
443 study) in the juvenile stage. FMRFamide-lir neurons and axons innervate the enteric nervous
444 system of juvenile annelids like *C. teleta* (15). At the same time, MIP is also present in the
445 stomatogastric nervous system in dinophilids (40), and it plays a role in the feeding behaviour

of *P. dumerilii* larva (50), suggesting a conserved neuropeptide-mediated control of feeding in annelids.

Conclusions

Our study describes the transition of the nervous system from the early larva to the adult stage in the annelid *O. fusiformis*, a representative of Oweniidae and the sister lineage to all remaining annelids. The initial larval neural system comprises an apical organ connected to a prototrochal ring and the chaetal sac through several neurites. Soon, a bilobed brain forms underneath the apical organ, connecting with other larval tissues and the developing juvenile trunk in its anterior part. During metamorphosis, the lobes, and the ventral and dorsal roots fuse to form a ring-shaped brain, following a similar trend of reorganisation of the neural architecture as in other "early branching" annelids like magelonids and chaetopterids (22, 25, 26). However, our findings indicate that the larval and adult nervous systems are not as simple as previously thought in *O. fusiformis* and retain similarities with more deeply nested annelids, particularly at the larval stages. Future studies of the detailed connectome of the mitraria larva will help to understand how these anatomical similarities translate into conservation of behaviours and physiological functions, illuminating how neuropeptidergic systems might have contributed to the evolution of biphasic life cycles.

List of abbreviations

als: anterio-lateral somata

an: anus

ao: apical organ

ar: apical nerve ring

471 at: apical tuft

472 br: brain

473 CLSM: confocal laser scanning microscopy

474 cc: circumesophageal connective

475 chn: chaetal sac nerve

476 co: collar

477 cs: chaetal sac

478 cts: ciliated thoracic segment

479 dn: dorsal nerve

480 dnc: dorsal nerve cord

481 dr: dorsal root

482 fg: foregut

483 fgn: foregut nerve

484 fn: frontal nerve

485 gz: growth zone

486 jr: juvenile rudiment

487 lc: lateral cord

488 lmc: lateral medullary cord

489 lml: lower mouth lip

490 ln: lateral transverse nerve

491 lpn: left peripheral nerve

492 mg: midgut

493 MIP: myoinhibitory peptide

494 mo: mouth

495 mt: mucous tube

ne: neurite

np: brain neuropil

nph: nephridia

pgo: parapodial glandular organ

pls: posterior-lateral somata

pr: prototrochal ring

pt: prototroch

so: somata

rg: refringet globule

rpn: right peripheral nerve

tc: tentacle crown

th: thorax

tp: tentacle plexus

vnc: ventral nerve cord

vr: ventral root

Declarations

Ethics approval and consent to participate

Not applicable.

Consent for publication

Not applicable.

Availability of data and materials

The datasets used and analysed during the current study are available from the corresponding author upon reasonable request.

Competing interests

The authors declare that they have no competing interests.

Funding

This study was funded by the Company of Biologists (Travel fellowship grant JEBTF2205748) to AMCB and the European Research Council (Starting Grant, Action number 801669) to JMMD.

Authors' contributions

AMCB and JMMD designed the study. AMCB and RD performed all the immunostainings and fluorescence imaging. AMCB performed the expression analyses and imaging of gene expression. EAW and GJ contributed with reagents and sequencing data. AMCB, RD and JMMD built the figures. AMCB drafted the manuscript. All authors contributed to data interpretation and manuscript writing.

Acknowledgements

We thank all members of the Martín-Durán lab for their support. We thank Océane Seudre for amplifying and synthesising the *soxC* probe and Paul Kalke for recommendations regarding immunostaining of the adult heads. We also thank the Station Biologique de Roscoff for their help with collections and animal supplies.

References

1. Jékely G, Keijzer F, Godfrey-Smith P. An option space for early neural evolution. Philos Trans R Soc Lond B Biol Sci. 2015;370(1684).

2. Bullock TH, Horridge GA. Structure and Function in the Nervous Systems of Invertebrates. San Francisco: W. H. Freeman and Company; 1965. 1719 p.

3. Martín-Durán JM, Hejnol A. A developmental perspective on the evolution of the nervous system. Dev Biol. 2021;475:181-92.

4. Hejnol A, Lowe CJ. Embracing the comparative approach: how robust phylogenies and broader developmental sampling impacts the understanding of nervous system evolution. Philos Trans R Soc Lond B Biol Sci. 2015;370(1684).

5. Northcutt RG. Evolution of centralized nervous systems: two schools of evolutionary thought. Proc Natl Acad Sci U S A. 2012;109 Suppl 1(Suppl 1):10626-33.

6. Hartenstein V, Stollewerk A. The evolution of early neurogenesis. Dev Cell. 2015;32(4):390-407.

7. Arendt D, Urzainqui IQ, Vergara HM. The conserved core of the nereid brain: Circular CNS, apical nervous system and lhx6-arx-dlx neurons. Curr Opin Neurobiol. 2021;71:178-87.

8. Liang Y, Carrillo-Baltodano AM, Martín-Durán JM. Emerging trends in the study of spiralian larvae. Evol Dev. 2023.

9. Martín-Durán JM, Pang K, Borve A, Le HS, Furu A, Cannon JT, et al. Convergent evolution of bilaterian nerve cords. Nature. 2018;553(7686):45-50.

10. Denes AS, Jékely G, Steinmetz PR, Raible F, Snyman H, Prud'homme B, et al. Molecular architecture of annelid nerve cord supports common origin of nervous system centralization in Bilateria. Cell. 2007;129(2):277-88.

570 11. Marlow H, Tosches MA, Tomer R, Steinmetz PR, Lauri A, Larsson T, et al. Larval body
571 patterning and apical organs are conserved in animal evolution. BMC Biology. 2014;12(7):1-
572 17.
573 12. Helm C, Beckers P, Bartolomaeus T, Drukewitz SH, Kourtesis I, Weigert A, et al.
574 Convergent evolution of the ladder-like ventral nerve cord in Annelida. Front Zool.
575 2018;15:36.
576 13. Purschke G. Annelida: Basal Groups and Pleistoannelida. In: Schmidt-Rhaesa A, Harzsch
577 S, editors. Structure and Evolution of Invertebrate Nervous Systems. Oxford: Oxford
578 University Press; 2016. p. 254-312.
579 14. Orrhage L, Müller CHG. Morphology of the nervous system of Polychaeta (Annelida).
580 Hydrobiologia. 2005;535/536:79-111.
581 15. Meyer NP, Carrillo-Baltodano A, Moore RE, Seaver EC. Nervous system development in
582 lecithotrophic larval and juvenile stages of the annelid *Capitella teleta*. Front Zool.
583 2015;12:15.
584 16. Vopalensky P, Tosches MA, Achim K, Handberg-Thorsager M, Arendt D. From spiral
585 cleavage to bilateral symmetry: the developmental cell lineage of the annelid brain. BMC
586 Biol. 2019;17(1):81.
587 17. Kumar S, Tumu SC, Helm C, Hausen H. The development of early pioneer neurons in the
588 annelid *Malacoceros fuliginosus*. BMC Evol Biol. 2020;20(1):117.
589 18. Sur A, Magie CR, Seaver EC, Meyer NP. Spatiotemporal regulation of nervous system
590 development in the annelid *Capitella teleta*. Evodevo. 2017;8:13.
591 19. McDougall C, Chen WC, Shimeld SM, Ferrier DE. The development of the larval
592 nervous system, musculature and ciliary bands of *Pomatoceros lamarckii* (Annelida):
593 heterochrony in polychaetes. Front Zool. 2006;3:16.

20. Starunov VV, Voronezhskaya EE, Nezlin LP. Development of the nervous system in *Platynereis dumerilii* (Nereididae, Annelida). Front Zool. 2017;14:27.

21. Purschke G, Vodopyanov S, Baller A, von Palubitzki T, Bartolomaeus T, Beckers P. Ultrastructure of cerebral eyes in Oweniidae and Chaetopteridae (Annelida) - implications for the evolution of eyes in Annelida. Zoological Lett. 2022;8(1):3.

22. Beckers P, Helm C, Purschke G, Worsaae K, Hutchings P, Bartolomaeus T. The central nervous system of Oweniidae (Annelida) and its implications for the structure of the ancestral annelid brain. Front Zool. 2019;16:6.

23. Helm C, Vocking O, Kourtesis I, Hausen H. *Owenia fusiformis* - a basally branching annelid suitable for studying ancestral features of annelid neural development. BMC Evol Biol. 2016;16(1):129.

24. Carrillo-Baltodano AM, Seudre O, Guynes K, Martín-Durán JM. Early embryogenesis and organogenesis in the annelid *Owenia fusiformis*. Evodevo. 2021;12(1):5.

25.Beckers P, Helm C, Bartolomaeus T. The anatomy and development of the nervous system in Magelonidae (Annelida) - insights into the evolution of the annelid brain. BMC Evol Biol. 2019;19(1):173.

26.Helm C, Schwarze G, Beckers P. Loss of complexity from larval towards adult nervous systems in Chaetopteridae (Chaetopteriformia, Annelida) unveils evolutionary patterns in Annelida. Organisms Diversity & Evolution. 2022;22(3):631-47.

27.Wilson DP. On the mitraria larva of *Owenia fusiformis* Delle Chiaje. Philosophical Transcations of the Royal Society B. 1932;221(474-482):231-334.

28. Smart TI, von Dassow G. Unusual development of the mitraria larva in the polychaete *Owenia collaris*. Biological Bulletin. 2009;217:253-68.

617 29. Martín-Zamora FM, Liang Y, Guynes K, Carrillo-Baltodano AM, Davies BE, Donnellan
618 RD, et al. Annelid functional genomics reveal the origins of bilaterian life cycles. Nature.
619 2023;615(7950):105-10.
620 30. Conzelmann M, Jékely G. Antibodies against conserved amidated neuropeptide epitopes
621 enrich the comparative neurobiology toolbox. Evodevo. 2012;3:23.
622 31. Conzelmann M, Offenburger SL, Asadulina A, Keller T, Munch TA, Jékely G.
623 Neuropeptides regulate swimming depth of *Platynereis* larvae. Proc Natl Acad Sci U S A.
624 2011;108(46):E1174-83.
625 32. Conzelmann M, Williams EA, Tunaru S, Randel N, Shahidi R, Asadulina A, et al.
626 Conserved MIP receptor-ligand pair regulates *Platynereis* larval settlement. Proc Natl Acad
627 Sci U S A. 2013;110(20):8224-9.
628 33. Martín-Durán JM, Passamaneck YJ, Martindale MQ, Hejnol A. The developmental basis
629 for the recurrent evolution of deuterostomy and protostomy. Nat Ecol Evol. 2016;1(1):5.
630 34. Seudre O, Carrillo-Baltodano AM, Liang Y, Martín-Durán JM. ERK1/2 is an ancestral
631 organising signal in spiral cleavage. Nat Commun. 2022;13(1):2286.
632 35. Müller J, Bartolomaeus T, Tilic E. Formation and degeneration of scaled capillary
633 notochaetae in *Owenia fusiformis* Delle Chiaje, 1844 (Oweniidae, Annelida).
634 Zoomorphology. 2021;141(1):43-56.
635 36. Rouse GW, Pleijel F, Tilic E. Oweniidae Rioja, 1917. In: Rouse GW, Pleijel F, TIlic E,
636 editors. Annelida. Oxford: Oxford University Press; 2022. p. 321-5.
637 37. Schnitzler C, Simmons DK, Pang K, Martindale MQ, Baxevanis AD. Expression of
638 multiple *Sox* genes through embryonic development in the ctenophore *Mnemiopsis leidyi* is
639 spatially restricted to zones of cell proliferation. Evodevo. 2014;5(15):1-17.
640 38. Price MN, Dehal PS, Arkin AP. FastTree 2--approximately maximum-likelihood trees for
641 large alignments. PLoS One. 2010;5(3):e9490.

642 39. Rueden CT, Schindelin J, Hiner MC, DeZonia BE, Walter AE, Arena ET, et al. ImageJ2:
643 ImageJ for the next generation of scientific image data. BMC Bioinformatics.
644 2017;18(1):529.
645 40. Kerbl A, Conzelmann M, Jékely G, Worsaae K. High diversity in neuropeptide
646 immunoreactivity patterns among three closely related species of Dinophilidae (Annelida). J
647 Comp Neurol. 2017;525(17):3596-635.
648 41. Müller MC. Polychaete nervous systems: Ground pattern and variations--cLS microscopy
649 and the importance of novel characteristics in phylogenetic analysis. Integr Comp Biol.
650 2006;46(2):125-33.
651 42. Rimskaya-Korsakova N, Dyachuk V, Temereva E. Parapodial glandular organs in
652 *Owenia borealis* (Annelida: Oweniidae) and their possible relationship with nephridia. J Exp
653 Zool B Mol Dev Evol. 2020;334(2):88-99.
654 43. Rimskaya-Korsakova NN, Kristof A, Malakhov VV, Wanninger A. Neural architecture of
655 *Galathowenia oculata* Zach, 1923 (Oweniidae, Annelida). Front Zool. 2016;13:5.
656 44. Temereva E, Rimskaya-Korsakova N, Dyachuk V. Detailed morphology of tentacular
657 apparatus and central nervous system in *Owenia borealis* (Annelida, Oweniidae). Zoological
658 Lett. 2021;7(1):15.
659 45. Veraszto C, Guhmann M, Jia H, Rajan VBV, Bezares-Calderón LA, Pineiro-Lopez C, et
660 al. Ciliary and rhabdomeric photoreceptor-cell circuits form a spectral depth gauge in marine
661 zooplankton. Elife. 2018;7.
662 46. Jokura K, Ueda N, Gühmann M, Yañez-Guerra LA, Słowiński P, Wedgwood KCA, et al.
663 Nitric oxide feedback to ciliary photoreceptor cells gates a UV avoidance circuit. Elife.
664 2023;12(RP91258):1-52.
665 47. Jékely G. Origin and early evolution of neural circuits for the control of ciliary
666 locomotion. Proc Biol Sci. 2011;278(1707):914-22.

667 48. Williams EA, Veraszto C, Jasek S, Conzelmann M, Shahidi R, Bauknecht P, et al.
668 Synaptic and peptidergic connectome of a neurosecretory center in the annelid brain. Elife.
669 2017;6.
670 49. Williams EA, Jékely G. Neuronal cell types in the annelid Platynereis dumerilii. Curr
671 Opin Neurobiol. 2019;56:106-16.
672 50. Williams EA, Conzelmann M, Jékely G. Myoinhibitory peptide regulates feeding in the
673 marine annelid *Platynereis*. Front Zool. 2015;12(1):1.
674 51. Shahidi R, Williams EA, Conzelmann M, Asadulina A, Veraszto C, Jasek S, et al. A
675 serial multiplex immunogold labeling method for identifying peptidergic neurons in
676 connectomes. Elife. 2015;4.
677 52. Veraszto C, Ueda N, Bezares-Calderon LA, Panzera A, Williams EA, Shahidi R, et al.
678 Ciliomotor circuitry underlying whole-body coordination of ciliary activity in the *Platynereis*
679 larva. Elife. 2017;6.
680 53. Seudre O, Martín-Zamora FM, Rapisarda V, Luqman I, Carrillo-Baltodano AM, Martín-
681 Durán JM. The *Fox* gene repertoire in the annelid *Owenia fusiformis* eveals multiple
682 expansions of the *foxQ2* class in Spiralia. Genome Biol Evol. 2022;14(10).
683 54. Jackson DJ, Meyer NP, Seaver E, Pang K, McDougall C, Moy VN, et al. Developmental
684 expression of *COE* across the Metazoa supports a conserved role in neuronal cell-type
685 specification and mesodermal development. Dev Genes Evol. 2010;220(7-8):221-34.
686 55. Carrillo-Baltodano AM, Boyle MJ, Rice ME, Meyer NP. Developmental architecture of
687 the nervous system in *Themiste lageniformis* (Sipuncula): New evidence from confocal laser
688 scanning microscopy and gene expression. J Morphol. 2019;280(11):1628-50.
689 56. Meyer NP, Seaver EC. Neurogenesis in an annelid: characterization of brain neural
690 precursors in the polychaete *Capitella* sp. I. Dev Biol. 2009;335(1):237-52.

691 57. Tomer R, Denes AS, Tessmar-Raible K, Arendt D. Profiling by image registration reveals
692 common origin of annelid mushroom bodies and vertebrate pallium. Cell. 2010;142(5):800-9.
693 58. Heuer CM, Müller CHG, Todt C, Loesel R. Comparative neuroanatomy suggests
694 repeated reduction of neuroarchitectural complexity in Annelida. Front Zool. 2010;7(13):1-
695 21.
696 59. Purschke G. On the ground pattern of Annelida. Organisms Diversity & Evolution.
697 2002;2(3):181-96.
698 60. Gustafsson MKS, Halton DW, Kreshchenko ND, Movsessian SO, Raikova OI, Reuter M,
699 et al. Neuropeptides in flatworms. Peptides. 2002;23(11):2053-61.
700 61. Beckers P, Loesel R, Bartolomaeus T. The nervous systems of basally branching
701 nemertea (Palaeonemertea). PLoS One. 2013;8(6):e66137.
702 62. Simakov O, Marletaz F, Cho SJ, Edsinger-Gonzales E, Havlak P, Hellsten U, et al.
703 Insights into bilaterian evolution from three spiralian genomes. Nature. 2013;493(7433):526-
704 31.
705
706 **Figure captions**
707
708 Figure 1. *Owenia fusiformis* development. **a** Developmental time course of stages studied:
709 gastrula, early larva, competent larva, metamorphosis, juvenile and adult. **b** Conserved motifs
710 in the epitopes of neuropeptides between *Platynereis dumerilii* (30-32) and *Owenia*
711 *fusiformis*. Representative mature peptides and conserved dipeptides are highlighted in red
712 and bold, respectively. **c** Cross-species reactivity tested across several annelids (30, 32, 40).
713
714 Figure 2. Neuropeptide-lir elements in the early mitraria. Confocal Laser Scanning
715 Microscopy (CLSM) images of DAPI (cyan), acetylated tubulin (yellow) and neuropeptide-

lir (red or white) elements at 24 hpf. All images are lateral views except for ventral views in **g**–**i**. Insets in (**b**, **e**, **i and k**) are close ups of the apical organ (ao) in the same view as the larger image. **a–c** FVamide-lir cells in the apical organ and one cell anterior to the foregut (white arrow). **d**–**i** RYamide-lir cells are present in the apical organ, with RYamide-lir axons (fn, dn, and orange arrowheads) connecting with seven RYamide-lir cells (magenta arrows) and an RYamide-lir prototrochal ring (pr). **j**–**l** RGWamide-lir cells are exclusively present in the apical organ. an: anus; ao: apical organ; at: apical tuft; cs: chaetal sac; dn: dorsal nerve; fg: foregut; fn: frontal nerve; mg: midgut; mo: mouth; pr: prototrochal ring; pt: prototroch.

Figure 3. Tubulin^{+} elements in the early mitraria. CLSM images of DAPI (cyan) and beta-tubulin (**a**–**j**) and alpha-acetylated tubulin (**k**–**m**) (yellow) at 24 hpf. Insets in (**f**–**g**) are close ups of the peripheral neuron in **e**. **a**–**c** Lateral views with beta-tubulin^{+} axons extending from the apical organ (ao) anteriorly (fn), dorsally (dn) and laterally (rpn, lpn; orange arrowheads) towards the prototroch ring. The polar bodies (pb) are still visible at this stage in the blastocoel space between the apical organ and the midgut (mg). Beta-tubulin is also staining the cell boundaries across the body of the larva, like in **c**. **d**–**g** Ventral views showing at least one beta-tubulin^{+} monociliated cell (magenta arrow) in the prototroch that presumably connects to the apical organ via a peripheral nerve (rpn1). **h**–**j** Two bilateral peripheral nerves (rpn1–rpn2 and lpn1–lpn2) branch out on each side of the episphere towards the tubulin^{+} prototrochal ring (pr). **k**–**m** Most of the beta-tubulin^{+} axons are also with acetylated tubulin. ao: apical organ; at: apical tuft; dn: dorsal nerve; fn: frontal nerve; lpn1–lpn2: left peripheral nerves 1–2; mg: midgut; mo: mouth; pr: prototrochal ring; pt: prototroch; rg: refringent globule; rpn1–rpn2: right peripheral nerves 1–2.

Figure 4. Neuropeptide-lir elements in the competent larvae. CLSM images of DAPI (cyan), acetylated tubulin (yellow) and neuropeptide-lir (red or white) elements in the competent larvae (~ 3 wpf). Apical views, with anterior to the top. **c**–**f**, **i**–**l**, **o**–**p** and **s**–**v** are close ups of the foregut or apical organ in the same view as the respective larger image in **b**, **h**, **n**, **r**. **a**–**b**, **e**–**f** FVamide-lir cells and **q**–**r**, **u**–**v** MIP-lir cells in the apical organ connect via FVamide-lir and MIP circumesophageal connectives (cc) to the ventral nerve cord (vnc) of the juvenile trunk rudiment (jr) (See Additional File 3: Supplementary Figure 3), and via **a**–**b** FVamide-lir, **g**–**h** RYamide-lir and **q**–**r** MIP-lir frontal (fn), dorsal (dn) and peripheral nerves (orange arrow heads) to the **a**–**b** FVamide-lir, **g**–**h** RYamide-lir and **q**–**r** MIP-lir prototrochal ring (pr). An **e**–**f** FVamide-lir, **i**–**j** RYamide-lir and **u**–**v** MIP-lir apical nerve ring (ar) surrounds the apical tuft. The foregut is innervated by **a**–**d** FVamide-lir cells and neurites. **k**–**l** RYamide-lir axons form a neuropil between two brain lobes (rbl–lbl) underneath the apical organ. **m**–**p** RGWamide-lir cells remain only in the apical organ. Arrow in **r**, **t** is presumably background staining.an: anus; ao: apical organ; ar: apical nerve ring; at: apical tuft; br: brain; cc: circumesophageal connectives; chn: chaetal sac nerve; cs: chaetal sac; dn: dorsal nerve; dr: dorsal root; fg: foregut; fgn: foregut nerve; fn: frontal nerve; jr: juvenile rudiment; mg: midgut; mo: mouth; np: brain neuropil; pr: prototrochal ring; pt: prototroch; vr: ventral root.

Figure 5 Expression of neural genes in the competent larvae. Differential Interference Contrast (DIC) images showing expression of *soxC*, *pou4*, *six3/6*, *otx*, *nk2.1* and *ChAt*. **a**, **c**, **e**, **g**, **i**, **k** lateral views; **b**, **d**, **f**, **h**, **j**, **l** apical views. Insets are close ups of the corresponding larger images in anterior view. All genes, except for *otx* **g**–**h**, have a bilateral expression in the brain (br). **a**–**b** *soxC* is strongly expressed in the juvenile rudiment (jr), the mouth (mo), and the anterior part of the foregut (fg). **g**–**l** *otx*, *nk2.1* and *ChAt* have some weaker expression in the foregut. **g**–**h** in addition *otx* is expressed in the prototroch. an: anus; br:

765 brain; cs: chaetal sac; fg: foregut; jr: juvenile rudiment; mo: mouth; pgo: parapodial glandular
766 organ; pt: prototroch.
767
768 Figure 6 Neuropeptide-lir elements during metamorphosis. CLSM images of DAPI (cyan)
769 and neuropeptide^{+} (red or white) elements during metamorphosis (~ 3-4 wpf). Ventral views,
770 with anterior to the top. **c**–**d**, **g**–**h**, **k**–**l**, **o**–**p** are close ups of the apical organ and brain in the
771 same view as the respective larger image in **a**–**b**, **e**–**f**, **i**–**j**, **m**–**n**. **a**–**b**, **e**–**f**, **i**–**j**, **m**–**n** The brain
772 connects with the ventral nerve cord (vnc), via circumesophageal connectives (lateral
773 medullary cords (22) at the trunk thorax, made out of three ciliated thoracis segments (cts).
774 Iterated **a–b** FVamide-lir, **e–f** RYamide-lir and **m–n** MIP-lir neurons and transverse lateral
775 nerves are present in the segments of the trunk. **i–j** RWG labels the parapodial glandular
776 organs (pgos). Double yellow line marks the division between thoracic and abdominal
777 segments. ao: apical organ; ar: apical nerve ring; br: brain; cc: circumesophageal connectives;
778 cts: ciliated thoracic segments; dr: dorsal root; fg: foregut; fgn: foregut nerve; lmc: lateral
779 medullary cords; lml: lower mouth lip; np: brain neuropil; pgo: parapodial glandular organ 1–
780 4; pr: prototrochal ring; pt: prototroch; vnc: ventral nerve cord; vr: ventral root.
781
782 Figure 7 Neural development during metamorphosis. DIC images showing expression of
783 *soxC*, *pou4*, *six3/6*, *otx*, *nk2.1* and *ChAt*. **a**, **c**, **e**, **g**, **i** Lateral views; **b**, **d**, **f**, **h**, **j**, ventral views.
784 Insets are close ups focusing on the brain of the corresponding larger images. **a–b** *soxC*, **e–f**
785 *six3/6* and **k–l** *ChAT* are expressed in the brain (br). **a–b** *soxC* is expressed throughout the
786 trunk, the foregut (fg), and in the putative growth zone (gz). **e–f** *six3/6* and i**–j** are expressed
787 on the dorsal side of the foregut, while **g–h** *otx* is expressed in the boundary between foregut
788 and midgut. an: anus; br: brain; cc: circumesophageal connectives; cts: ciliated thoracic
789 segments; dr: dorsal root; fg: foregut; fgn: foregut nerve; lmc: lateral medullary cords; lml:

790 lower mouth lip; np: brain neuropil; pgo: parapodial glandular organ 1–4; pr: prototrochal
791 ring; pt: prototroch; vnc: ventral nerve cord; vr: ventral root.
792
793 Figure 8 Neuropeptide-lir elements in the juveniles. CLSM images of DAPI (cyan) and
794 neuropeptide-lir (red or white) elements in juveniles (>4 wpf). **a**, **c**, **e**, **g** Ventral views; **b**, **d**,
795 **f**, **h** lateral views, with anterior to the top. The brain connects with the ventral nerve cord
796 (vnc), via circumesophageal connectives (lateral medullary cords (22) at the trunk thorax,
797 made out of three ciliated thoracic segments (cts). Iterated **a–b** FVamide-lir, **c–d** RYamide-lir
798 and **g–h** MIP-lir neurons and lateral transverse nerves (ln) are present in the segments of the
799 trunk. **e–f** RWG labels the parapodial glandular organs (pgos). Double yellow line marks the
800 division between thoracic and abdominal segments. br: brain; cc: circumesophageal
801 connectives; cts: ciliated thoracic segments; lmc: lateral medullary cords; lml: lower mouth
802 lip; mo: mouth; mt: mucous tube; pgo: parapodial glandular organ 1–4; vnc: ventral nerve
803 cord.
804
805 Figure 9. Neuropeptide-lir elements in the head of adults. CLSM images of DAPI (cyan) and
806 neuropeptide-lir (red or white) elements. **a, c, e, g** ventral views; **b, d, f, h** dorsal views. **a, c,**
807 **e, g** The FVamide-lir, RYamide-lir, RGWamide-lir and MIP-lir brain ring (br) is connected
808 via lateral medullary cords (lmc) to the ventral nerve cord (vnc) at the position of the thorax
809 (th). Each tentacle of the head contains a basiepidermal nerve plexus (tp), which projects
810 from the brain. **b, d, f, h** Posterior to the head there is a dorsal nerve plexus (dnp).
811 Surrounding each eye are clusters of somata oriented in an anterior-lateral (als) and
812 posterior-lateral position (pls) position, showing FVamide-lir, RYamide-lir, and MIP-lir. als:
813 anterio-lateral somata; br: brain; ch: chaetae; co: collar; dorsal nerve plexus: dnp; ey: eye;

814 lmc: lateral medullary cord; lml: lower mouth lip; pls: posterior-lateral somata; tc: tentacle
815 crown; th: thorax; tp: tentacle plexus; vnc: ventral nerve cord.
816
817 Figure 10. Diagram of neural development in *O. fusiformis*. **a** At 24 hpf there is an FVamide-
818 lir, RYamide-lir, RGWamide-lir, MIP-lir and FMRFamide-lir apical organ with *elav*$^{+}$ and
819 *synaptotagmin*$^{+}$ cells that connect to the prototroch ring (24). **b** The brain goes from a bilobed
820 brain in the pre-competent larvae, to a ring in the juvenile **c** Pattern of immunoreactivity and
821 *soxC* and *six3/6* expression in the juvenile. ao: apical organ; as: abdominal segment; at: apical
822 tuft; br: brain; ch: chaetae; cs: chaetal sac; cts: ciliated thoracic segment; dn: dorsal nerve;
823 dnc: dorsal nerve cord; dr: dorsal root; fn: frontarl nerve; gz: growth zone; lc: lateral cord;
824 lmc: lateral medullary cords; lpn: left peripheral nerve; mg: midgut; pgo: parapodial
825 glandular organ; pr: prototroch ring; pt: prototroch; rbl: right brain lobe; rpn: right peripheral
826 nerve; vr: ventral root.
827
828 Supplementary Figure 1 Alignment of the neuropeptide precursors *P. dumerilii* (30-32), *C.*
829 *teleta* (62) and *Owenia fusiformis* (29). Representative mature peptides and conserved
830 dipeptides are highlighted in red and bold, respectively.
831
832 Supplementary Figure 2 MIP-lir elements in the 24hpf mitraria. MIP-lir cells include several
833 cells as part of the apical organ (ao) and one cell anterior to the foregut (white arrow),
834 including a MIP-lir frontal nerve (fn). Inset in **b** is a close up of the apical organ (ao) in the
835 same view as the larger image. ao: apical organ; at: apical tuft; cs: chaetal sac; fn: frontal
836 nerve; mo: mouth.
837

838 Supplementary Figure 3. Neuropeptide-lir elements in the competent larvae. CLSM images
839 of DAPI (cyan), acetylated tubulin (yellow) and neuropeptide-lir (red or white) elements in
840 the competent larvae (~ 3 wpf). Lateral views, with anterior to the left. **c**, **f**, **i**, **l** are close ups
841 of the juvenile rudiment in the same view as the respective larger image in **b**, **e**, **h**, **k**. **a–c**
842 FVamide-lir cells and MIP-lir cells in the apical organ connect via FVamide-lir and MIP-lir
843 circumesophageal connectives (cc) to the ventral nerve cord (vnc) of the juvenile trunk
844 rudiment (jr), and via **a–b** FVamide-lir, **d–e** RYamide-lir and **j–k** MIP-lir frontal (fn), dorsal
845 (dn) and peripheral nerves (closed orange arrow heads) to the **a–c** FVamide-lir, **d–f**
846 RYamide-lir and **j–l** MIP-lir prototrochal ring (pr). See also Figure 2. **d–f** RYamide-lir and **j–**
847 **l** MIP-lir peripheral nerves also branch out to the chaetal nerve (chn) (open pink arrowheads).
848 The foregut is innervated by **a–c** FVamide-lir and **d–f** RYamide-lir cells and neurites. By this
849 stage the juvenile rudiment has a vnc and a **a–c** FVamide-lir and **d–f** RYamide-lir dorsal
850 nerve cord (dnc). **g–i** RGWamide-lir cells are only present in the apical organ. **j–l** MIP-lir is
851 present in the anterior part of the foregut (white arrow). an: anus; ao: apical organ; at: apical
852 tuft; br: brain; cc: circumesophageal connectives; chn: chaetal sac nerve; cs: chaetal sac; dn:
853 dorsal nerve; dnc: dorsal nerve cord; fg: foregut; fgn: foregut nerve; fn: frontal nerve; jr:
854 juvenile rudiment; mg: midgut; mo: mouth; pr: prototrochal ring; pt: prototroch; vnc: ventral
855 nerve cord.
856
857 Supplementary Figure 4 Tubulin^{+} elements in the competent. CLSM images of beta-tubulin
858 (**a–e**) and alpha-acetylated tubulin (**f–j**) in the competent larvae (~3 wpf). **a–c**, **g–h** apical
859 views; **d–e**, **i–j**, lateral views; **f** ventral view. **a–c**, **g–h** the apical organ (ao), associated with
860 an apical tuft (at) and apical nerve ring (ar) is positioned above the brain (br). Ventral (vr)
861 and dorsal (dr) roots **c**, **h** make the neuropil of the brain, that connects with the **d**
862 cirucomesophageal connectives (cc), and ultimately with the ventral nerve cord (vnc) **d–e**. **f**,

863 **i–j** Tubulin^{+} peripheral nerves (fn, dn, and orange arrowheads) connect the apical organ with
864 the prototroch ring (pr). ao: apical organ; an: anus; ar: apical nerve ring; at: apical tuft; br:
865 brain; cb: chaetoblast; cc: circumesophageal connectives; chn: chaetal sac nerve; cs: chaetal
866 sac; dn: dorsal nerve; dnc: dorsal nerve cord; dr: dorsal root; fg: foregut; fgn: foregut nerve;
867 fn: frontal nerve; jr: juvenile rudiment; mg: midgut; mo: mouth; nph: nephridia; pr:
868 prototrochal ring; pt: prototroch; vnc: ventral nerve cord; vr: ventral root.
869
870 Supplementary Figure 5 SoxC orthology and early mRNA expression. **a** Maximum likelihood
871 orthology assignments of *soxC*. **b** DIC images showing expression of *soxC* during
872 gastrulation (9hpf) and early mitraria (24hpf). Asterisks mark the animal/apical pole an: anus;
873 bp: blastopore; cs: chaetal sac; fg: foregut; mo: mouth; pt: prototroch.
874
875 Supplementary Figure 6 Neuropeptide-lir elements during metamorphosis. CLSM images of
876 DAPI (cyan) and neuropeptide-lir (red or white) elements during metamorphosis (~ 3 4pf).
877 Lateral views, with anterior to the top. **a–h**The brain connects with the ventral nerve cord
878 (vnc), via circumesophageal connectives (lateral medullary cords (22) at the trunk thorax,
879 made out of three ciliated thoracis segments (cts). The foregut (fg) has **b** FVamide-lir, **f**
880 RYamide-lir and **h** MIP-lir neurons and cells. **e–f** RWGamide labels the parapodial glandular
881 organs (pgos), and the lower mouth lip (lml). Double yellow line marks the division between
882 thoracic and abdominal segments. ao: apical organ; an: anus; br: brain; cc: circumesophageal
883 connectives; cts: ciliated thoracic segments; dn: dorsal nerve; dr: dorsal root; fg: foregut; fgn:
884 foregut nerve; lmc: lateral medullary cords; lml: lower mouth lip; np: brain neuropil; pgo:
885 parapodial glandular organ 1–4; pr: prototrochal ring; pt: prototroch; vnc: ventral nerve cord;
886 vr: ventral root.
887

888 Supplementary Figure 7 Tubulin^{+} elements during metamorphosis and juvenile. CLSM
889 images of acetylated tubulin. **a–b** Larvae undergoing metamorphosis. **c–d** >4 wfp juvenile.
890 **a–b** Tub^{+} peripheral nerves (orange arrowheads) in the remaining episphere of the larva keep
891 connecting the brain to the prototrochal ring (pr). **a–d** The brain connects with the ventral
892 nerve cord (vnc), via circumesophageal connectives (lateral medullary cords (22) at the trunk
893 thorax, made out of three ciliated thoracis segments (cts). The vnc is composed of two robust
894 longintudinal tracts, and two more lateral tracts (magenta arrows). On the anterior border of
895 each segment, there is a pair of lateral transverse nerves (ln) that connect to lateral ventral-
896 lateral longitudinal cords (magenta arrows). Double yellow line marks the division between
897 thoracic and abdominal segments. ao: apical organ; br: brain; cc: circumesophageal
898 connectives; cts: ciliated thoracic segments; dr: dorsal root; fn: frontarl nerve; lmc: lateral
899 medullary cords; ln: lateral transverse nerves; nph: nephridia; pr: prototrochal ring; pt:
900 prototroch; vnc: ventral nerve cord; vr: ventral root.
901
902 Supplementary Figure 8 Neural development in juveniles. DIC images showing expression of
903 *soxC*, *pou4*, *six3/6* and *otx*. **a**, **d**, **g**, **j** Lateral views; **b**, **e**, **h**, **k** ventral views; **c**, **f**, **i**, **l** dorsal
904 views. **a–c** *soxC* and **d–f** *six3/6* are expressed in the brain (br). **g–i** *pou 4* and **j–l** *otx* have no
905 longer any neural expression. **a–c** *soxC* is expressed in the foregut (fg), and in the putative
906 growth zone (gz). br: brain; fg: foregut; gz: growth zone; mo: mouth.
907
908 Supplementary Figure 9 Neuropeptide-lir elements in the adults. CLSM images of
909 neuropeptide-lir close ups of images in Figure 9. **a–b, e–f, i–j, m–n** ventral views; **c–d, g–h,**
910 **k–l**, **o–p** dorsal views. **a, e, i, m** Views of the eye showing FVamide-lir, RYamide-lir and
911 MIP-lir, antero-lateral (als) and postero-lateral (pls) somata. **b**, **f**, **j**, **n** Lateral head neurites
912 (lhn) extend toward the tentacles and the trunk. **c**, **g**, **k**, **o** Longitudinal dorsal nerve cord

(dnc). **d**, **h**, **l**, **p** Brain ring with associated neurites (ne) and somata (so). als: anterior-lateral somata; br: brain; dnc: dorsal nerve cord; ey: eye; lhn: lateral head neurites; lmc: lateral medullary cord; ne: neurite; pls: posterior-lateral somata; so: somata; tp: tentacle plexus.

Figure 1

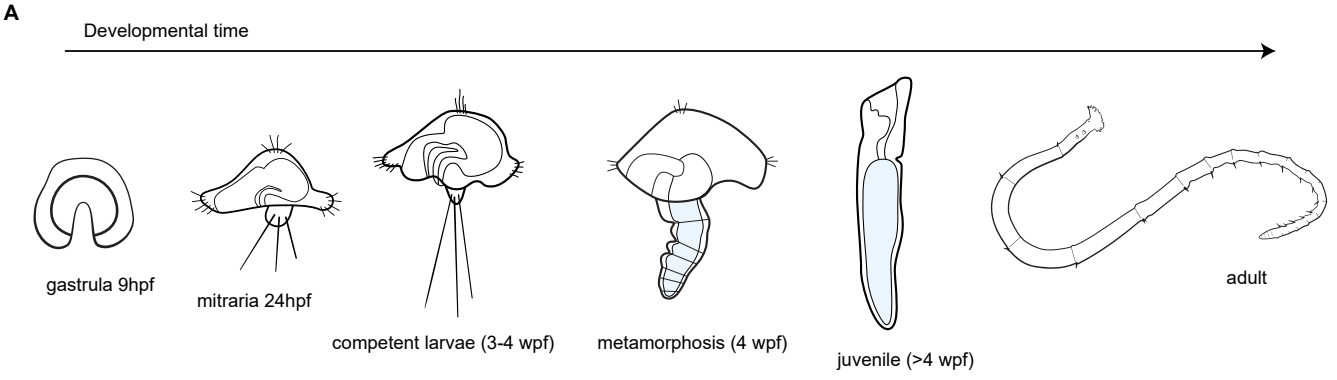
A
Developmental time
gastrula 9hpf
mitraria 24hpf
competent larvae (3-4 wpf)
metamorphosis (4 wpf)
juvenile (>4 wpf)
adult
B
FV
P. dumerilii FVamide precursor AEE25642.1
K R P H N F V G K R
O. fusiformis FVamide precursor CAH1786749.1
K R R N M F V G K R
RY
P. dumerilii RYamide precursor AEE25645.1
K R G T L M R Y G K R
O. fusiformis RYamide precursor CAH1772730.1
K R Q S F M R Y G K R
RGW
P. dumerilii RGWamide precursor AFS33094.1
K R R G W G K R
O. fusiformis RGWamide precursor CAH1783991.1
K R R G W G K R
MIP2
P. dumerilii MIP precursor AFV92893.1
K R G W K Q G A S Y S W G K R
O. fusiformis MIP precursor CAH1786447.1
K R A W Q N P G S -- W G K R
C
cross-species immunoreactivity
FV
RY
RGW
MIP2
Capitella teleta
Platynereis dumerilii
Trilobodrilus axi
Dinophilus taeniatus
Dimorphilus gyrociliatus
Owenia fusiformis
?

Figure 2

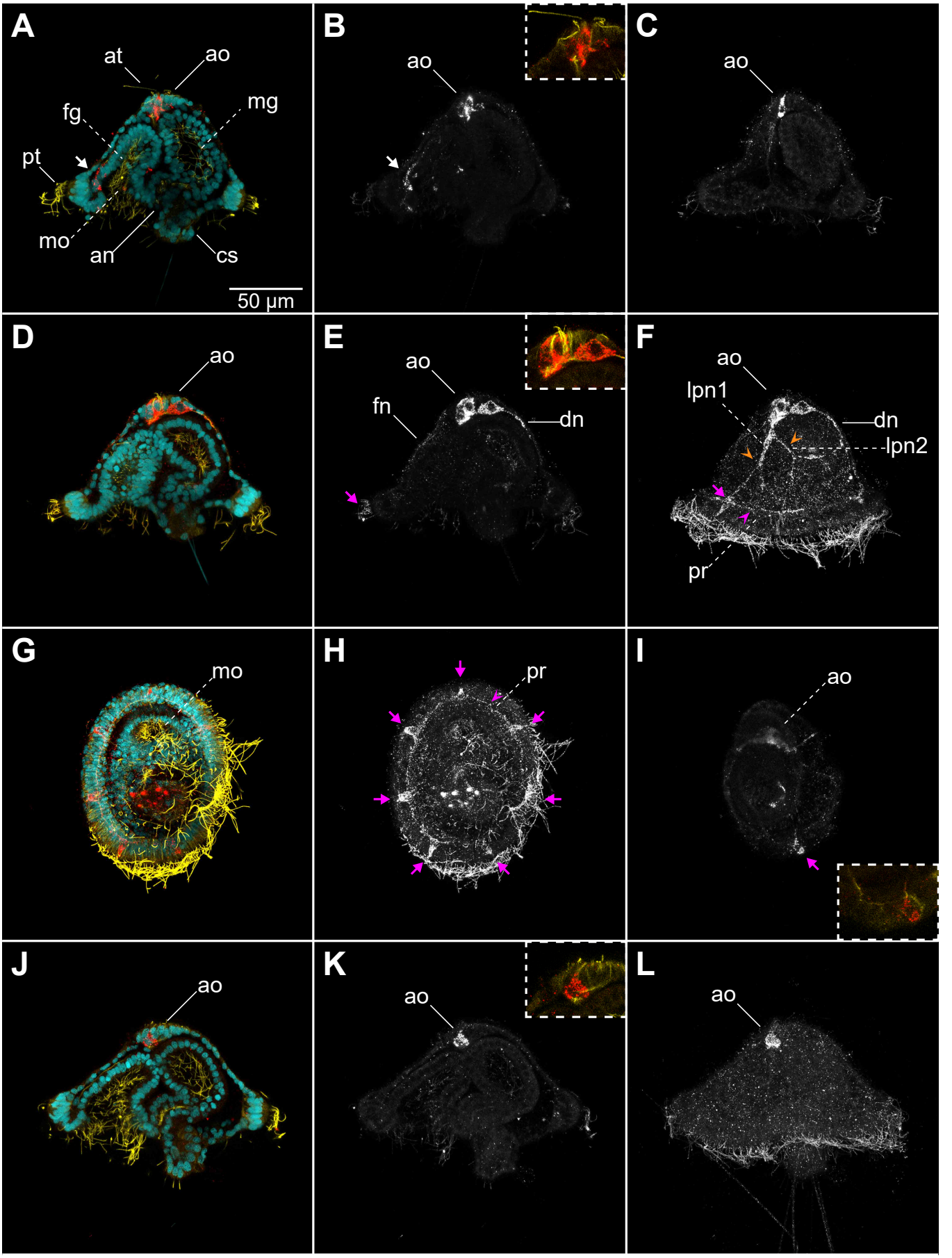
FVamide-lir
RYamide-lir
RGWamide-lir
A
at
ao
mg
fg
pt
mo
an
cs
50 µm
B
ao
C
ao
D
ao
E
ao
fn
dn
F
ao
lpn1
dn
lpn2
pr
G
mo
H
pr
I
ao
J
ao
K
ao
L
ao

Figure 3

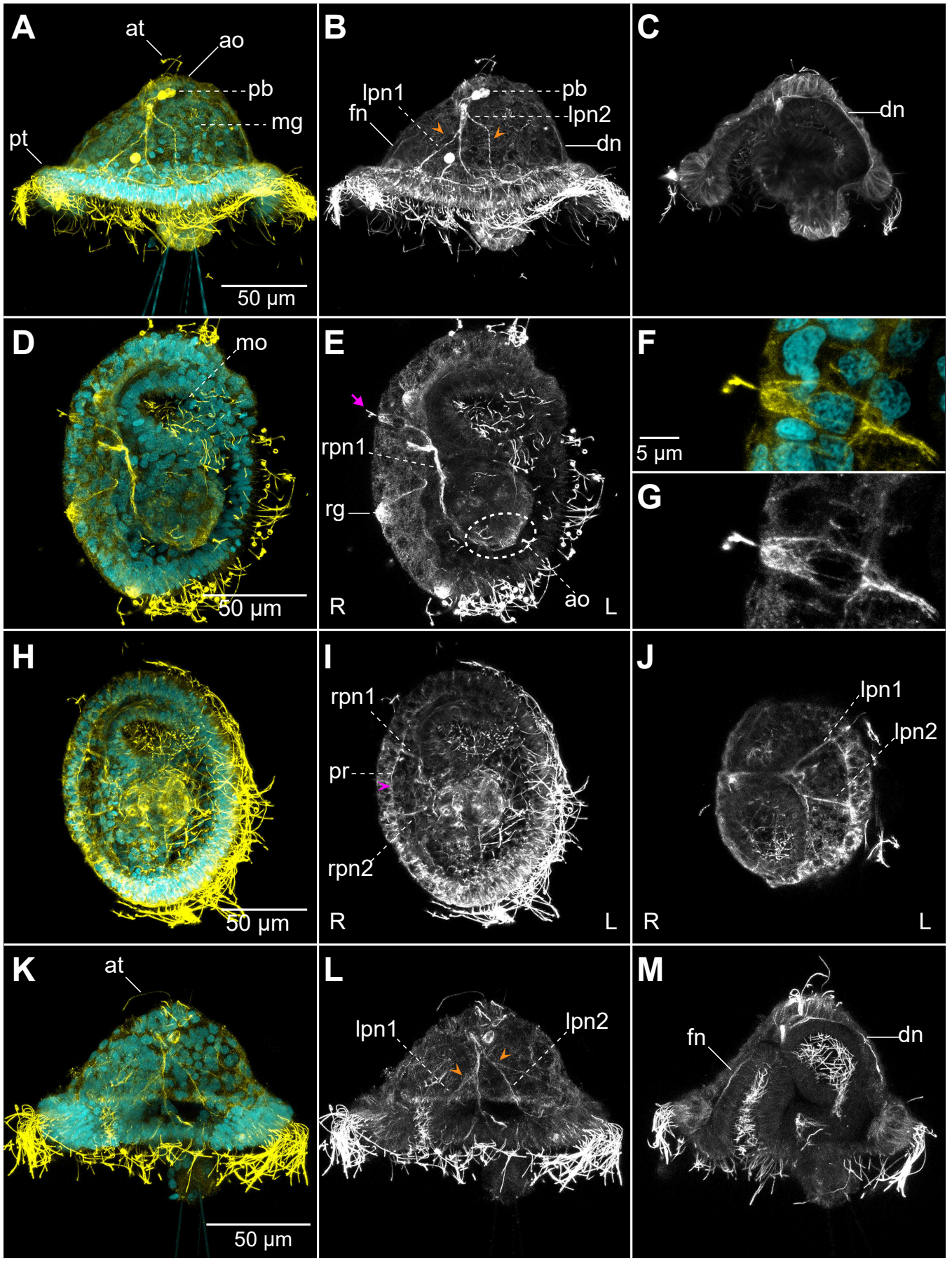
beta tubulin
alpha acetylated tubulin
A
at
ao
pb
mg
pt
50 µm
B
lpn1
fn
pb
lpn2
dn
C
dn
D
mo
50 µm
E
rpn1
rg
R
ao
L
F
5 µm
G
H
50 µm
I
rpn1
pr
rpn2
R
L
J
lpn1
lpn2
R
L
K
at
50 µm
L
lpn1
lpn2
M
fn
dn

Figure 4

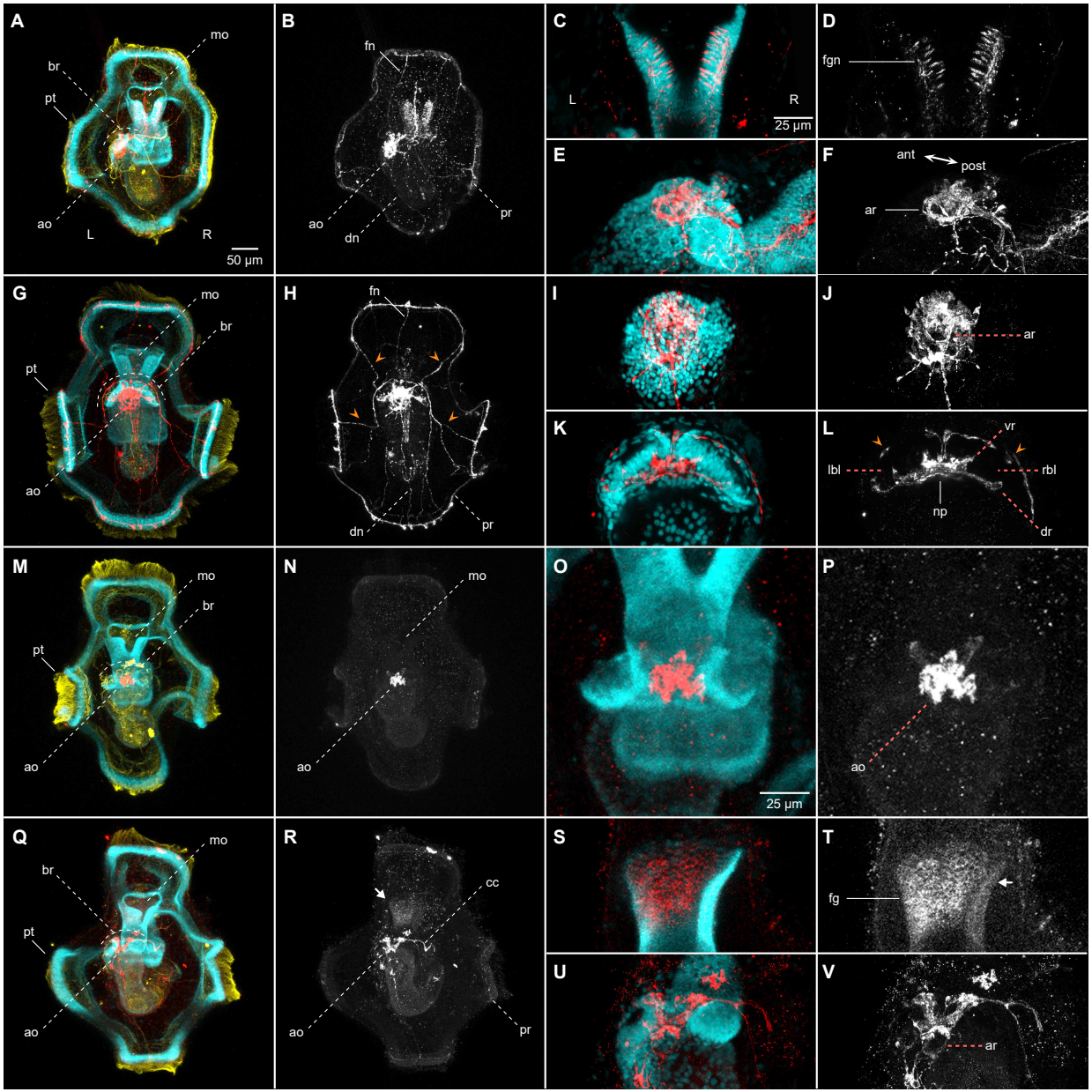
FVamide-lir
RYamide-lir
RGWamide-lir
MIP-lir
A
mo
br
pt
ao
L
R
50 µm
B
fn
ao
dn
pr
C
L
R
25 µm
D
fgn
E
F
ant
post
ar
G
mo
br
pt
ao
H
fn
dn
pr
I
J
ar
K
L
vr
lbl
rbl
np
dr
M
mo
br
pt
ao
N
mo
ao
O
25 µm
P
ao
Q
mo
br
pt
ao
R
cc
ao
pr
S
T
fg
U
V
ar

Figure 5

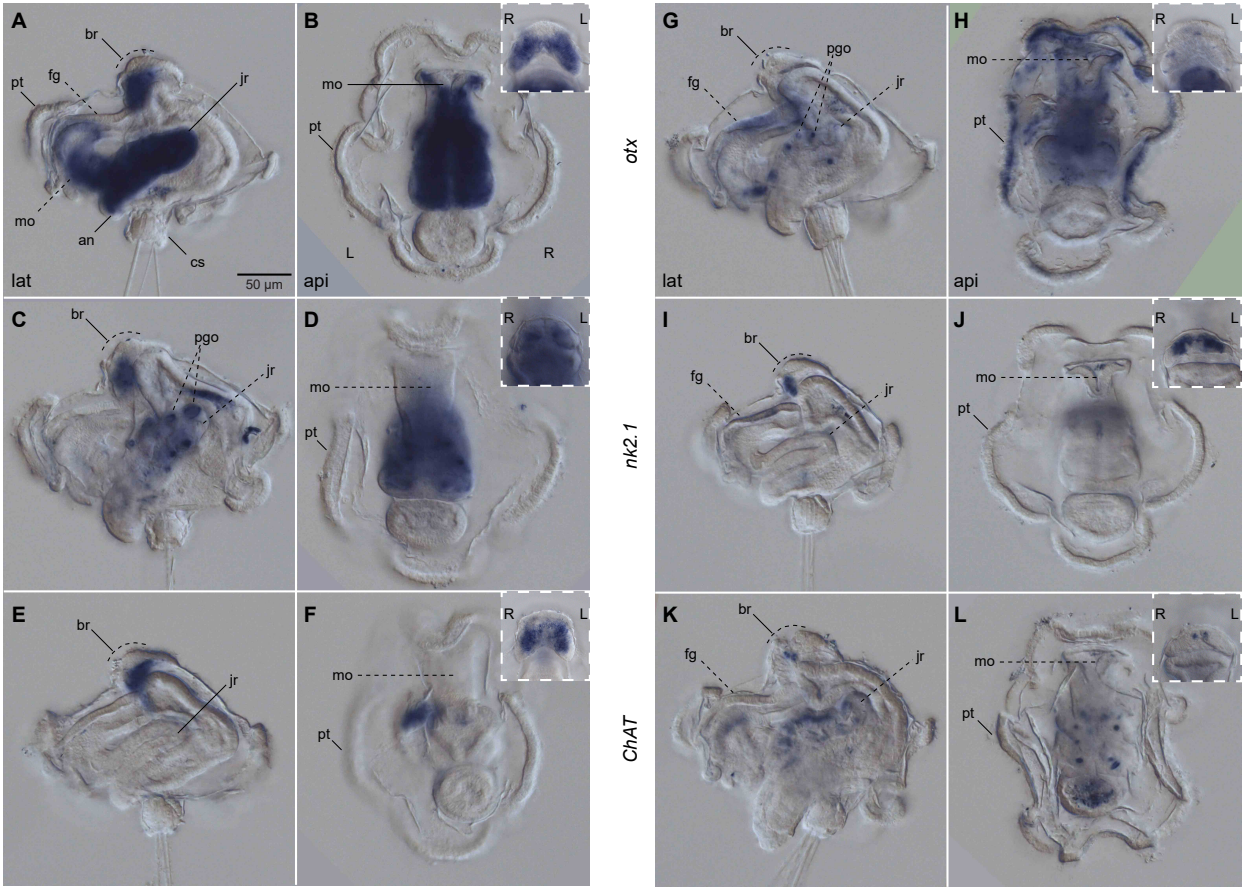
soxC
pou4
six3/6
otx
nk2.1
ChAT
A
B
C
D
E
F
G
H
I
J
K
L
br
fg
jr
pt
mo
an
cs
pgo
R
L
lat
api
50 µm

Figure 6

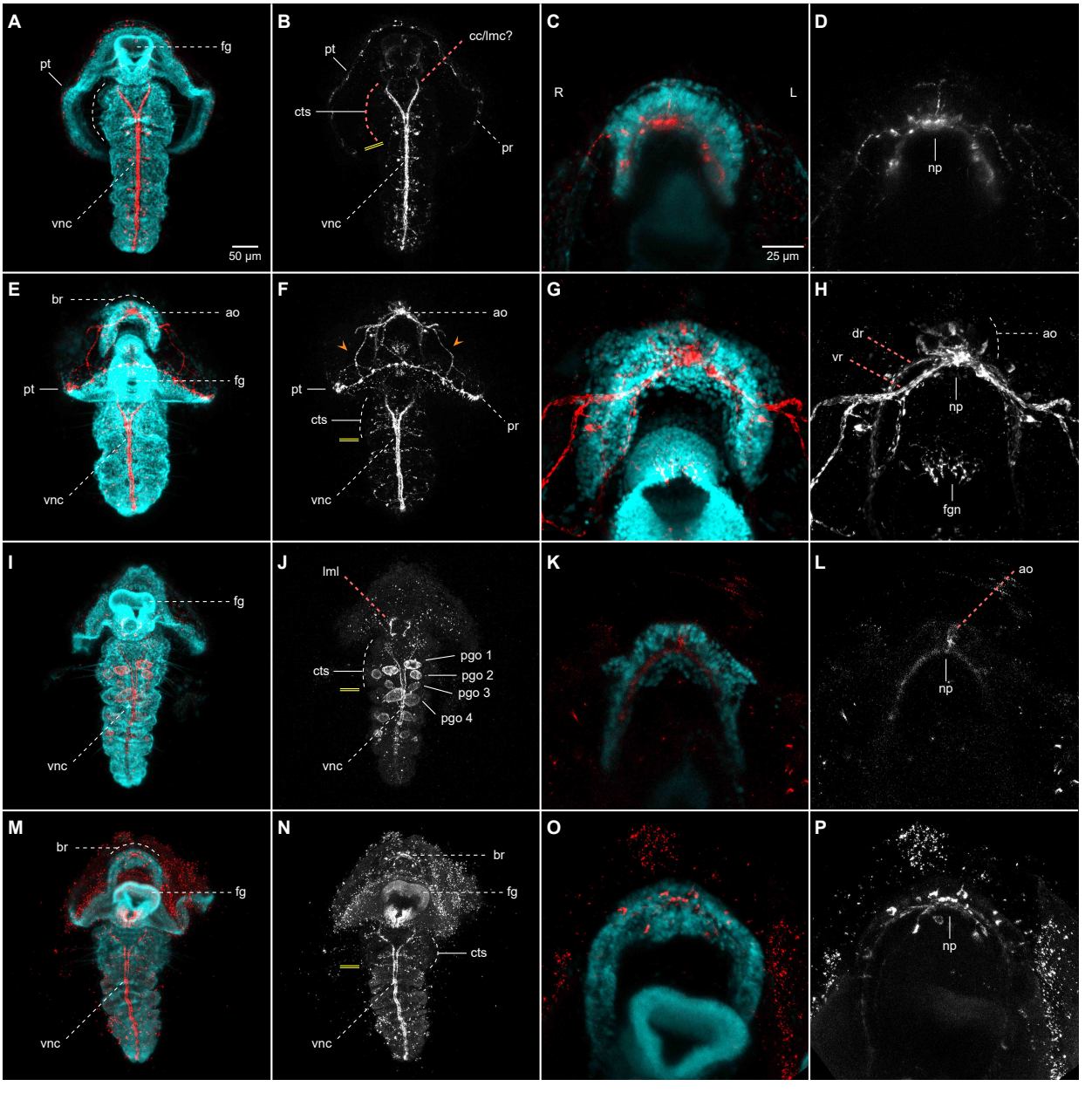
FVamide-lir
RYamide-lir
RGWamide-lir
MIP-lir
A
B
C
D
E
F
G
H
I
J
K
L
M
N
O
P
pt
fg
vnc
50 µm
cc/lmc?
cts
pr
R
L
25 µm
np
br
ao
dr
vr
fgn
lml
pgo 1
pgo 2
pgo 3
pgo 4

Figure 7

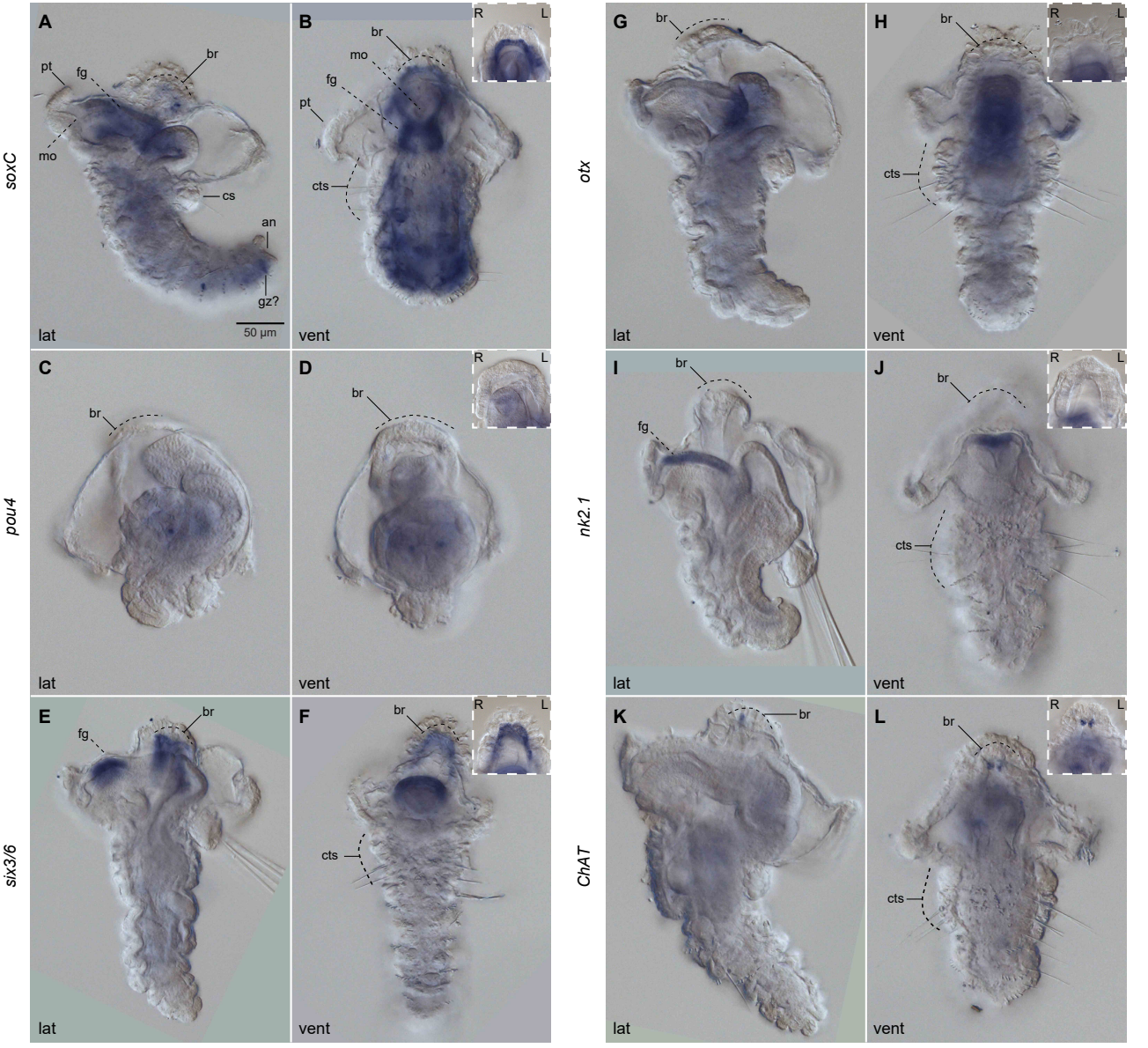
soxC
otx
pou4
nk2.1
six3/6
ChAT
A
B
C
D
E
F
G
H
I
J
K
L
pt
fg
br
mo
cs
an
gz?
cts
R
L
lat
vent
50 µm

Figure 8

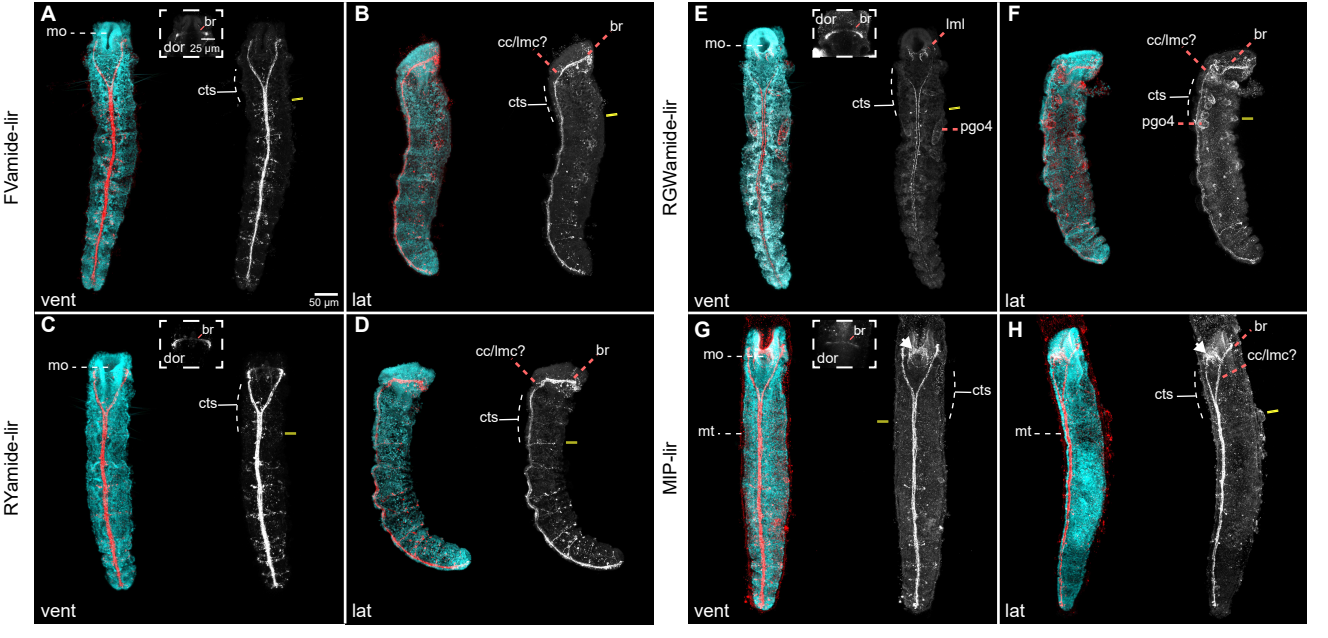
FVamide-lir
RYamide-lir
RGWamide-lir
MIP-lir
A
mo
br
dor
25 µm
cts
vent
50 µm
B
cc/Imc?
br
cts
lat
C
mo
br
dor
cts
vent
D
cc/Imc?
br
cts
lat
E
mo
dor
br
lml
cts
pgo4
vent
F
cc/Imc?
br
cts
pgo4
lat
G
mo
br
dor
cts
mt
vent
H
br
cc/Imc?
cts
mt
lat

Figure 9

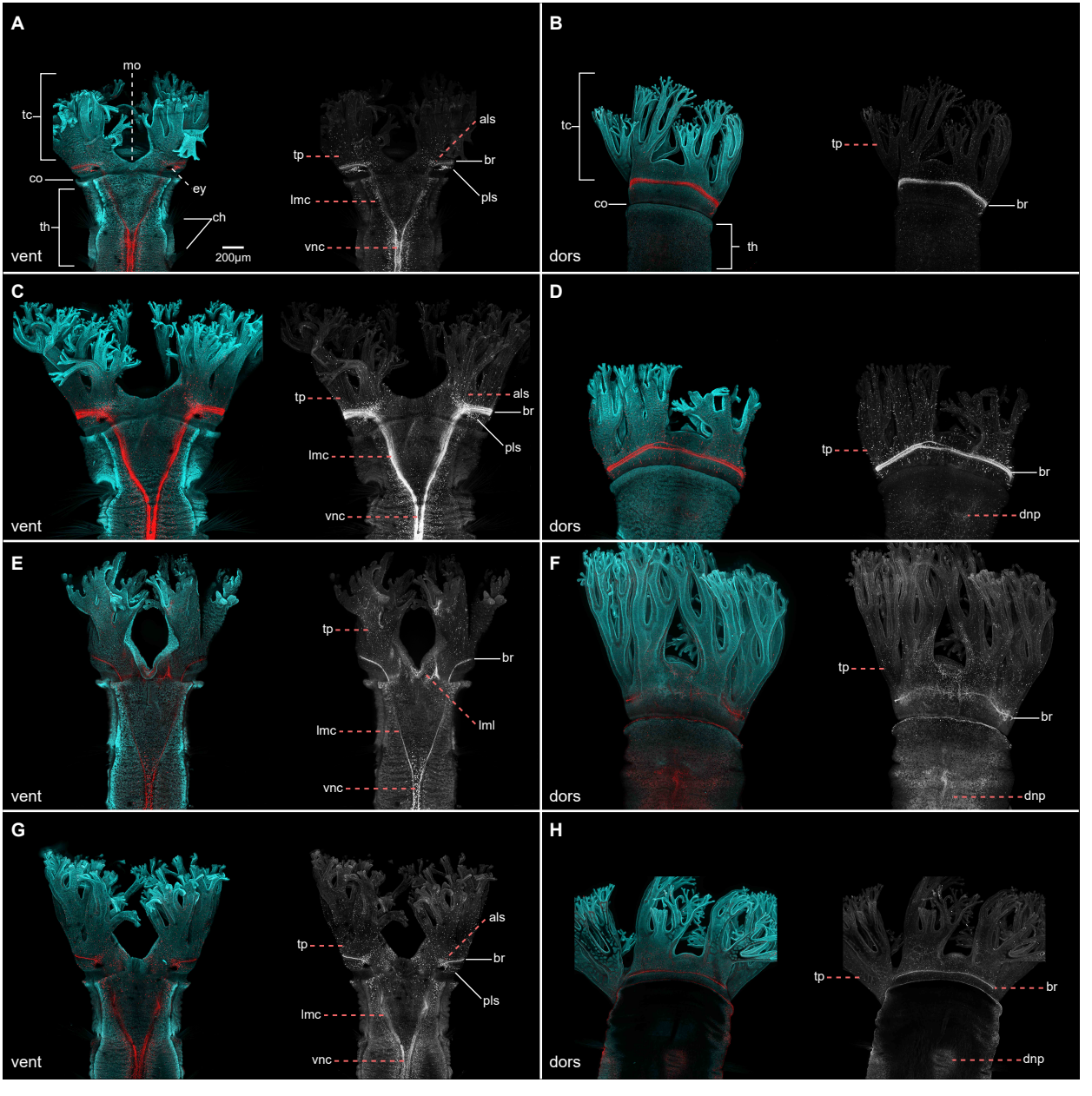
FVamide-lir
RYamide-lir
RGWamide-lir
MIP-lir
A
mo
tc
co
th
ey
ch
vent
200µm
tp
als
br
pls
lmc
vnc
B
tc
co
th
dors
tp
br
C
vent
tp
als
br
pls
lmc
vnc
D
dors
tp
br
dnp
E
vent
tp
br
lml
lmc
vnc
F
dors
tp
br
dnp
G
vent
tp
als
br
pls
lmc
vnc
H
dors
tp
br
dnp

Figure 10

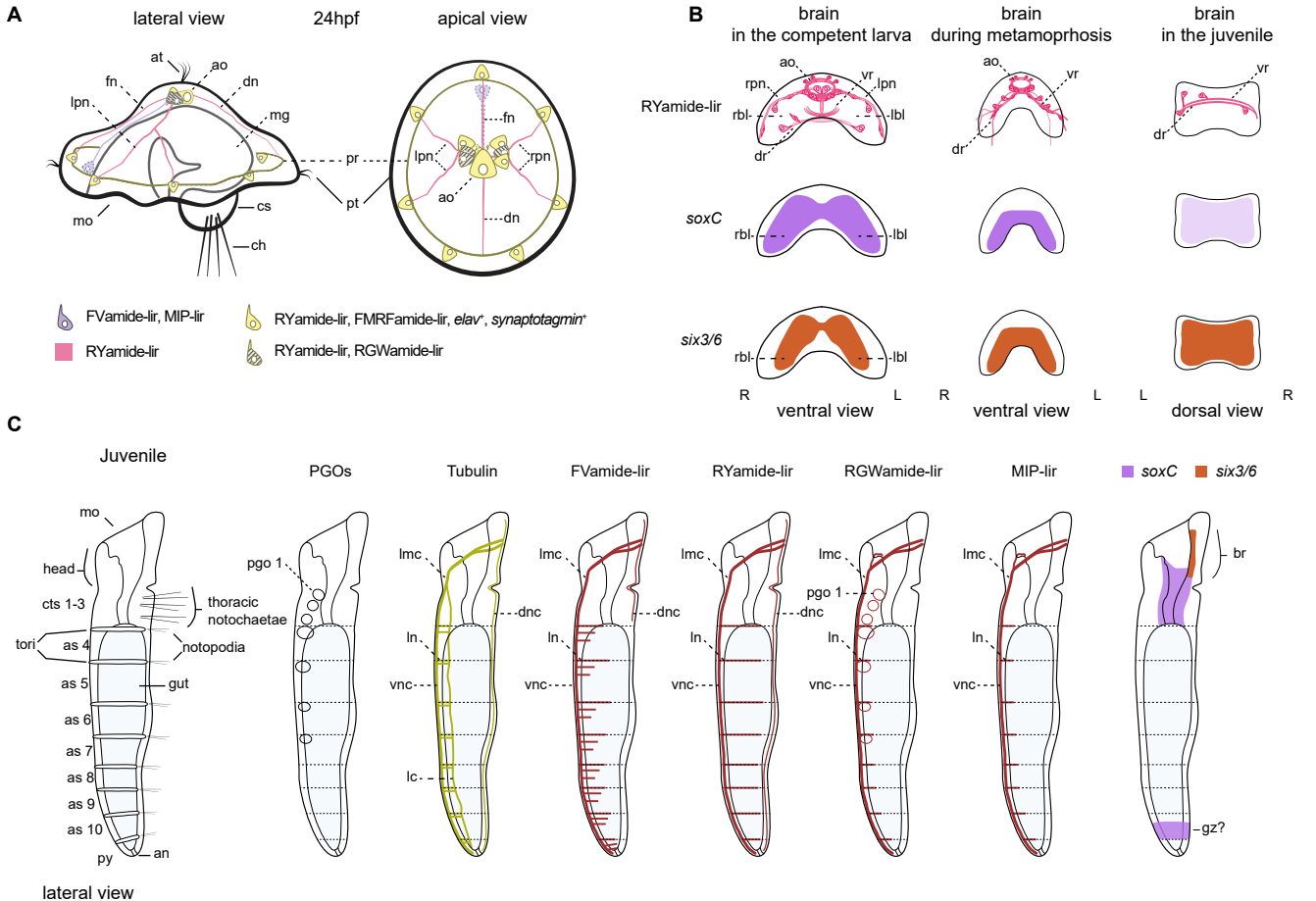
A
lateral view
24hpf
apical view
at
ao
dn
fn
lpn
mg
pr
pt
mo
cs
ch
rpn
FVamide-lir, MIP-lir
RYamide-lir
RYamide-lir, FMRFamide-lir, elav+, synaptotagmin+
RYamide-lir, RGWamide-lir
B
brain
in the competent larva
brain
during metamoprhosis
brain
in the juvenile
RYamide-lir
soxC
six3/6
vr
rbl
lbl
dr
R
L
ventral view
dorsal view
C
Juvenile
PGOs
Tubulin
FVamide-lir
RYamide-lir
RGWamide-lir
MIP-lir
soxC
six3/6
mo
head
cts 1-3
tori
as 4
as 5
as 6
as 7
as 8
as 9
as 10
py
an
thoracic
notochaetae
notopodia
gut
lateral view
pgo 1
lmc
ln
vnc
dnc
lc
br
gz?